

Simulation of a Passively Modelocked All-Fiber Laser
with Nonlinear Optical Loop Mirror

by
Joseph Shoer

Professor Jefferson Strait, Advisor

A thesis submitted in partial fulfillment
of the requirements for the
Degree of Bachelor of Arts with Honors
in Physics

WILLIAMS COLLEGE
Williamstown, Massachusetts

10 May 2006

Abstract

This thesis reports the development of a numerical simulator for the temporal pulse profiles produced by a passively modelocked all-fiber laser with a nonlinear optical loop mirror (NOLM). This simulator is capable of reproducing experimentally autocorrelated pulse shapes as well as mimicking experimentally observed general trends. We have used the simulator to confirm that our laser should produce soliton-like pulses and to explain a number of previously mysterious pulse shapes including a background offset in autocorrelations.

Contents

Chapter 1. Introduction	4
Chapter 2. Background	7
2.1 Pulse Propagation in Optical Fibers	7
2.2 Solitons	8
2.3 Experimental All-Fiber Laser	9
2.4 NOLM Power Transfer Curves	12
2.5 Diagnostic Measurements	15
Chapter 3. Components of the Simulator	18
3.1 Optical Fibers	18
3.2 NOLM Pulse Shaping	20
3.3 Laser Gain	22
3.4 Program Structure	24
Chapter 4. Results and Discussion	28
4.1 Experimental Results	28
4.2 Simulator Results: Pulse Profiles	32
4.3 Simulator Results: Polarization-Dependent Trends	38
Chapter 5. Conclusion	45
Appendix	48

Chapter 1. Introduction

The subject of this thesis is a new numerical model for a passively modelocked all-fiber pulse laser. In the future, this laser will be used as a test bed to investigate the propagation of short light pulses through optical communications fibers. Such pulses, on the order of a picosecond or less in duration, could form the basis of a high bit rate optical communications system. The laser is constructed entirely out of fiber components. It is modelocked by a nonlinear optical loop mirror (NOLM), a device consisting of a fiber loop and a coupler. Investigating and quantifying the behavior of the laser with mathematical models has been the thrust of research on this laser system for the past few years.

We are particularly interested in whether or not this laser's pulses are solitons or close to solitons. Soliton pulse shapes are of interest in optical communications because they do not experience dispersion-induced broadening like, for example, square pulses. In a data stream using light pulses to represent digital bits, dispersion can cause a pulse to broaden until its electric field envelope overlaps with that of the next pulse in the signal, increasing the chance of transmission errors unless the signal is regenerated at regular intervals. Using solitons to transmit data could drastically reduce this need for repeater stations. In fact, unbroadened soliton propagation has been demonstrated over effectively unlimited distances.¹

Before this fiber laser system can be used as a test bed to study the propagation of solitons over long distances of fiber, the laser must be thoroughly characterized. Previous work has produced a model that accounts for the role of polarization inside the NOLM fiber, which contributes to the modelocking behavior of the laser.² Now that we have a practical model to predict whether or not the laser will modelock, we need to investigate pulse shaping that occurs within the fiber cavity to predict the pulse shapes that the laser will produce. Current laboratory measurements of pulse shape use autocorrelation, which only gives us indirect information about pulse profiles, so more tools are needed to accurately describe the pulse shapes. We also need a way to determine how the polarization of light within the NOLM influences the temporal profile of the output pulses, since we observe several different pulse shapes depending on the NOLM polarization. Finally, we want to explain any deviations our pulses show from a soliton shape.

This thesis describes the development of a numerical simulator that effectively models the pulse-shaping devices present in the fiber laser cavity. The simulator, built on the *Mathematica* platform, explicitly takes into account the actions of the NOLM, soliton-shaping mechanisms in optical fibers, and gain-related effects on a temporal pulse profile. Simulation results compare well with experimentally observed pulse profiles, both in terms of specific pulse shapes and overall trends depending on the polarization of

light within the NOLM. In fact, the simulator has demonstrated that our laser can be expected to produce pulses that are very close to solitons in shape. Additionally, we have found the pulse shaping mechanisms built into the simulator to be sufficient to explain non-soliton structure found in experimental laser pulses. These background structures had no adequate explanation until now.

In Chapter 2, we present theoretical and practical background material. We will review the subject of pulse propagation in optical fibers, introduce soliton pulse shapes, and describe the experimental laser system. Chapter 3 will take readers step by step through each piece of the numerical simulator. We will describe the operation of each pulse-shaping mechanism in the laser, separately and in concert. We will present and discuss the important results of this simulator in Chapter 4, along with complementary experimental results. The simulator developed for this work has already proven to mimic laboratory behavior closely and will be a valuable tool for future investigations involving all-fiber lasers containing an NOLM or similar nonlinear device.

References

¹ Nakazawa, M., Y. Kamada, H. Kubota, and E.Suzuki. 10 Gbit/s soliton data transmission over one million kilometers. *Electronics Letters*, 27, 1270-1272 (1991); cited in Ferreira, M. F., *et al.* Optical solitons in fibers for communications systems. *Fiber and Integrated Optics*, 24, 287-313 (2005)

² Murray, Aubryn. Effects of polarization in a fiber laser with a nonlinear optical loop mirror. Thesis, Williams College, 2005

Chapter 2. Background

2.1 Pulse Propagation in Optical Fibers

The propagation of an optical pulse in a fiber, consisting of a high-index core surrounded by low-index cladding, is a complex if well-documented problem in physics. We must take two important effects into account to describe the behavior of light in silica glass fibers. First, glass is a dispersive medium, in which the speed of light waves depends on their frequency. A short pulse of light is composed of a Fourier sum of light waves with many different frequencies. Dispersion, then, tends to broaden short pulses in optical fibers. This effect can cause errors in data transmission systems using light pulses to represent digital bits because, over distance, the pulses will begin to overlap one another. Second, glass fibers have a nonlinear index of refraction. We can write the index as an intensity-dependent Taylor expansion:

$$n = n_0 + n_2|E|^2 + \dots \quad (2.1)$$

The second-order term (involving the *Kerr coefficient*, n_2) in this expansion leads to *self-phase modulation* (SPM), an intensity-dependent phase shift acquired by light propagating in the fiber. SPM causes more intense light to travel slower than less intense light. In a light pulse, the leading edge of the pulse (which rapidly increases in intensity) experiences an increasing index of refraction, slowing the cycles of light under the envelope and effectively inducing a redshift. The trailing edge experiences a falloff in intensity, a corresponding falloff in refractive index, and an effective blueshift. The combination gives pulse envelopes a frequency chirp; that is, the center frequency of the pulse increases across the pulse profile.

In order to describe the propagation of a light pulse including the effects of dispersion and nonlinearity, we must look at an optical fiber as a cylindrical waveguide. We can describe the behavior of light waves traveling through this waveguide by solving Maxwell's Equations in cylindrical coordinates. In particular, we are interested in the propagation of a pulse electric field envelope E that varies slowly compared to the frequency of the light. The result of this calculation is the nonlinear Schrödinger equation, a partial differential equation expressing E in terms of its spatial and temporal derivatives:^{1, 2}

$$i \frac{\partial E}{\partial z} + \frac{1}{2} \beta_2 \frac{\partial^2 E}{\partial t^2} + \gamma |E|^2 E = 0. \quad (2.2)$$

β_2 is a measure of the dispersion of the fiber, $\gamma = \frac{\omega_0}{c} n_2$ is the fiber nonlinearity parameter, z is the distance of propagation along the fiber, and time t is measured in the frame of the moving pulse. The second term in Equation 2.2 expresses the effect of dispersion in the optical fiber. The third term on the left-hand side of Equation 2.2 takes the nonlinearity of optical fibers into account. We can scale the nonlinear Schrödinger equation (or NLSE) and write it in terms of dimensionless quantities as

$$i \frac{\partial u}{\partial \xi} + \frac{1}{2} \frac{\partial^2 u}{\partial \tau^2} + |u|^2 u = 0. \quad (2.3)$$

Now, $u = E/E_0$ measures the pulse electric field envelope in dimensionless units, $\xi = z/l_d$ is the distance of propagation in terms of fiber *dispersion lengths* (also referred to as *soliton lengths*), and $\tau = t/t_0$ is dimensionless time delay in the frame of the moving pulse. The scaling factors for these dimensionless units are

$$\begin{aligned} E_0 &= \sqrt{n_2 \omega_0 l_d / 2c} \\ l_d &= t_0^2 / \beta_2 \\ t_0 &= \text{soliton width} \end{aligned} \quad (2.4)$$

where n_2 is the nonlinear Kerr coefficient, ω_0 is the carrier frequency of the pulse, and c is the speed of light. In this scaling scheme, the fundamental soliton width is fixed at an arbitrary value we choose while the other scaling factors depend on t_0 . In the simulations reported, we chose $t_0 = 1$ ps based on previous estimates of laser pulse widths.

2.2 Solitons

Dispersion and SPM act simultaneously in optical fibers. In the anomalous dispersion regime where β_2 is negative, higher-frequency (“bluer”) light travels faster than lower-frequency (“redder”) light, effectively blueshifting the leading edge of a pulse and redshifting the trailing edge. Optical fibers such as those in our laser cavity are typically operated near a wavelength of minimum attenuation, about 1.55 μm , which is in the anomalous dispersion regime ($\lambda > 1.312 \mu\text{m}$ for single-mode fibers).³ The intensity-dependent chirp induced by self-phase modulation, on the other hand, has the opposite effect as dispersion. Thus, SPM can balance anomalous dispersion for appropriate intensity profiles. These pulse shapes are called *solitons* because of their particle-like characteristics. Solitons, for example, can collide with one another, fall into bound states, and interact in other ways that suggest particles. The feature of solitons of greatest interest in the field of fiber optic communications is their ability to propagate stably without broadening. Using solitons to transmit digital bits could decrease the need for

repeater stations in fiber transmission lines and reduce the frequency of data transmission errors as communications pulses will not broaden and merge into one another.

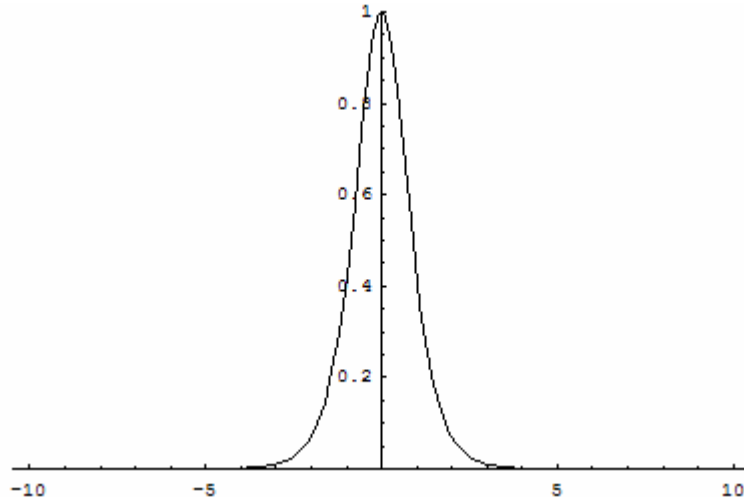


Figure 2.1 Intensity envelope of a first-order soliton, a hyperbolic secant squared. Horizontal axis is time in dimensionless units; vertical axis is intensity in dimensionless units.

The pulse shape of a soliton can be found by applying the inverse scattering method to Equation 2.3. The resulting pulse envelope is

$$u(\tau) = \eta \operatorname{sech}(\eta\tau), \quad (2.5)$$

where η is referred to as the *order* of the soliton. First order solitons have the special property of maintaining their hyperbolic secant shape, shown in Figure 2.1, as they propagate. (Higher order solitons undergo periodic variations in shape, but always return to their original temporal profile after each soliton length l_d .) There is a direct link between soliton peak intensity and width even within a single order: the shorter a soliton's duration, the larger its peak will be. This behavior, which is not readily apparent from Equation 2.5 when η is fixed, is built into the scaling factors t_0 and E_0 .⁴

Since only the first-order soliton retains its original shape over any distance of propagation, it is the soliton order of greatest utility for fiber optic communications. Therefore, we are concerned with the behavior of first-order solitons exclusively. The remainder of this thesis will use the term *soliton* to refer to first-order ($\eta = 1$) solitons, also called fundamental solitons.

2.3 Experimental All-Fiber Laser

Our laboratory work utilizes an all-fiber pulse laser constructed by previous thesis students.⁵ The laser cavity, diagrammed in Figure 2.2, is a figure-eight formed entirely of optical fibers and fiber optic components. Rather than using mirrors to reflect the beam through the gain medium many times, fiber forms a closed loop around the gain medium with output coupled directly out of the loop through a fiber coupler that removes

10% of the light from the cavity. Laser components are connected by splicing their fiber “pigtailes” together.

The primary lobe of the laser cavity (left side of Figure 2.2) is comprised of approximately 15 m of fiber. We have used SMF-28, a standard silica glass communications fiber that supports only the TEM₀₀ mode. The NOLM (nonlinear optical loop mirror, discussed below) is a loop approximately 78 m in length and is composed of dispersion-shifted fiber (DSF). DSF has been engineered to have near-zero dispersion at typical fiber communication wavelengths. This laser operates at 1.55 μm, a wavelength at which signal attenuation in silica glass fibers is at a minimum.

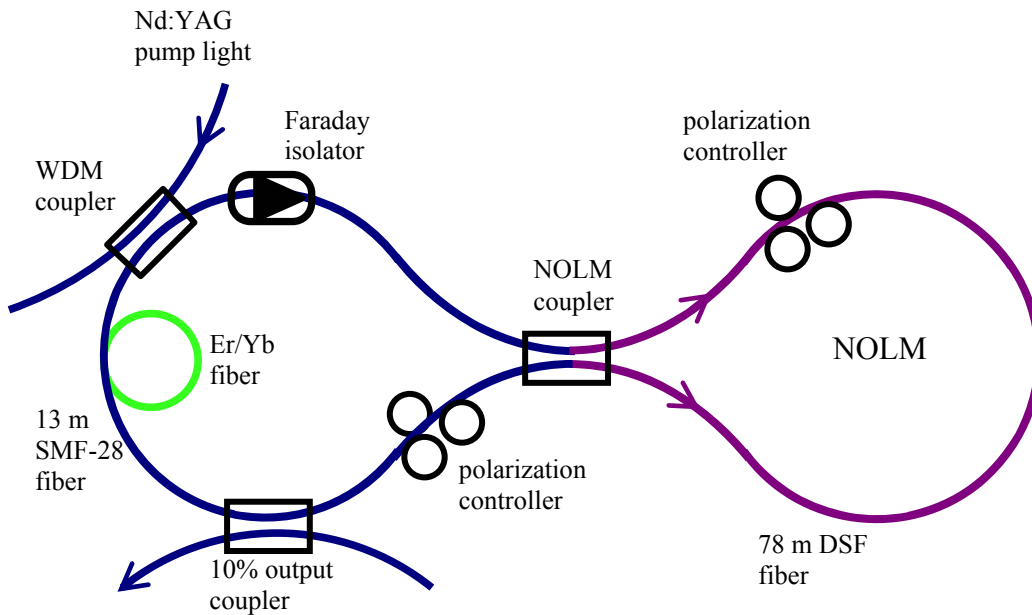


Figure 2.2 Fiber laser diagram. Solid lines represent optical fibers. See text for full explanation of fiber components.

The gain medium is a section of fiber doped with erbium and ytterbium ions. Pump light at 1.06 μm from a commercial Nd:YAG laser is injected into the fiber loop through a wavelength division multiplex (WDM) coupler that preferentially transmits 1.06 μm light across the coupler while allowing very little 1.55 μm laser light out of the fiber loop. The pump light excites a ${}^2F_{7/2} \rightarrow {}^2F_{5/2}$ transition in the ytterbium, which immediately transfers its energy into a population inversion in the erbium atoms, bringing them to the ${}^4I_{11/2}$ state. The erbium atoms then decay to the metastable state ${}^4I_{13/2}$ via phonon emission. The 1.55 μm lasing transition occurs from ${}^4I_{13/2} \rightarrow {}^4I_{15/2}$.

The direction of propagation of photons emitted by the erbium is limited by a Faraday isolator. The isolator is a fiber optic component that takes advantage of optical activity and a series of linear polarizers to act as a one-way gate for light in the fiber loop. We have positioned the Faraday isolator in the laser cavity to limit 1.55 μm light to one direction of travel around the loop. Since the isolator includes linear polarizers, it introduces a loss into the cavity depending on the polarization of the input light.

In order to maximize the throughput of the isolator, we optimize laser operation by ensuring that light entering the Faraday isolator closely matches the linear polarization of the first polarizer in the isolator. We achieve this using a polarization controller that consists of a quarter wave plate, a half wave plate, and another quarter wave plate in sequence. With this combination of optical elements, we can obtain any desired polarization from an arbitrary input by rotating the wave plate angles. In order to incorporate wave plates into the fiber cavity without introducing bulk optics, we take advantage of the fact that *bending* an optical fiber produces stress that induces birefringence in the fiber, with fast and slow axes oriented parallel and perpendicular to the direction of bending.⁶ The wave plates each consist of a paddle on a swivel mount. We have wrapped optical fiber around the paddles; three turns for the quarter wave plates and six turns for the half wave plate. When operating (and simulating) the laser, we assume that the polarization controller preceding the Faraday isolator is always set to align light with the isolator.

The nonlinear optical loop mirror, or NOLM, is a fiber component of simple construction that we use to modelock the fiber laser. Proposed by Doran and Wood in 1988,⁷ a NOLM is created by connecting two pigtails of a fiber coupler together with a loop of optical fiber (Figure 2.3). The particular feature of the NOLM we are interested in is its power response, which takes advantage of the nonlinearity of optical fibers.

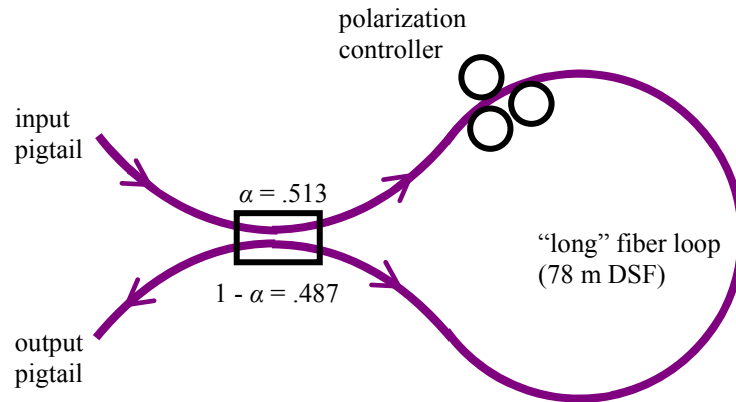


Figure 2.3 NOLM, consisting of a fiber coupler with two pigtails connected by a fiber loop. The coupler splits a light beam arriving on the input pigtail into two beams with relative electric field amplitudes α and $(1-\alpha)$, which travel in opposite directions around the loop.

The transmission of a light beam through the loop mirror from the input pigtail to the output depends on the splitting ratio α of the coupler. If $\alpha = 0.5$, then the NOLM acts as a reflector. Light will be evenly split into two counterpropagating beams, with one beam acquiring a $\pi/2$ phase shift when it crosses the coupler. After the beams have circulated around the loop, they interfere at the output pigtail. The beam that crosses the coupler again acquires a phase shift of $\pi/2$, so that when the beams combine, one has a total phase shift of zero while the other has been shifted by π . No light is seen at the

output, and by conservation of energy, all the light reflects back to the input (hence the term “loop *mirror*”).

Our NOLM incorporates a coupler with a splitting ratio of $\alpha = 0.513$. With slightly different intensities of light traveling in opposite directions around the loop, we must take into account the effects of the nonlinear index of refraction in optical fibers,

$$n = n_0 + n_2|E|^2 + \dots \quad (2.6)$$

In the case of a light wave entering the input pigtail, the nonlinear index of refraction causes the more intense beam to propagate through the loop at a slower speed. Thus, the unequal splitting ratio introduces an intensity-dependent differential phase shift between the two beams. The fiber loop is long in order to allow this phase to build up. We can construct a *power transfer curve* (abbreviated PTC) to capture the dependence of NOLM transmission on the input intensity. In their original proposal, Doran and Wood ignored the polarization of light within the NOLM and arrived at the PTC shown in Figure 2.4A.

We use the input power dependent transmission of the NOLM to modelock the fiber laser. Passive modelocking is the result of interrupting any laser cavity with a nonlinear device that preferentially transmits high intensities. If the laser can minimize its loss by increasing beam intensity, but the population inversion is not sufficient to simply increase continuous-wave (cw) intensity, then all the laser cavity modes will tend to “lock” together such that their Fourier sum is a pulse train. This process takes place as random intensity noise on a cw laser beam gets preferentially amplified at the expense of the less intense background.⁸ When the pump laser is activated, our laser is initially in cw operation. Introducing acoustic noise into the cavity by tapping the lab table initiates the process of modelocking. The fiber laser produces pulses on the order of one picosecond in duration, usually with one pulse per round trip of the laser cavity.

A pulse traveling through an optical fiber is subject to dispersion and nonlinearity. 1.55 μm is in the anomalous dispersion regime for silica glass, so the fibers in our laser can support soliton pulses. Indeed, if any pulse with energy equal to or exceeding that of a fundamental soliton propagates in an optical fiber, it should evolve into a soliton due to the actions of dispersion and SPM.⁹ Therefore, we believe that the fiber laser should produce soliton-like pulses when it modelocks. As we shall see in Chapter 4, the influence of other pulse shaping mechanisms in the fiber cavity cause the laser to produce pulses that are close to, but not quite, solitons.

2.4 NOLM Power Transfer Curves

In 2004-2005, Aubryn Murray did significant work to characterize power transfer curves, their effect on the NOLM, and their role in causing the laser to modelock.¹⁰ The fiber laser does not have a single PTC; the polarization of light inside the NOLM complicates the system. Since the power transfer curve depends on interference at the NOLM coupler, we can manipulate the PTC by changing the relative polarizations of the counterpropagating beams in the loop. In particular, a polarization mismatch between the recombining beams can alter the depth of modulation of the power transfer curve since waves of identical polarization interfere while waves of crossed polarization do not. Additionally, changing the polarization of beams in the NOLM can alter the phase of the

PTC because, if the counterpropagating beams travel along different birefringent axes in the fiber, their phases will differ when they recombine at the coupler. Two example PTCs are shown in Figure 2.4B. A polarization controller manipulates the polarization of light in the NOLM. We can rotate the wave plates to any desired combinations of angles between 0° and 180° , which we represent as an ordered triplet (ρ, φ, θ) . In our investigations, we leave the second quarter wave plate set at $\theta = 0^\circ$ and absorb any phase delay it contributes into a “mystery wave plate” that also accounts for birefringence induced by bending the remaining NOLM fiber around its spool. This reduces the polarization variables to the pair (ρ, φ) , which we think of as defining a polarization space where each point corresponds to a unique set of polarizations and a unique power transfer curve. The polarization space is periodic in each dimension with period 180° .

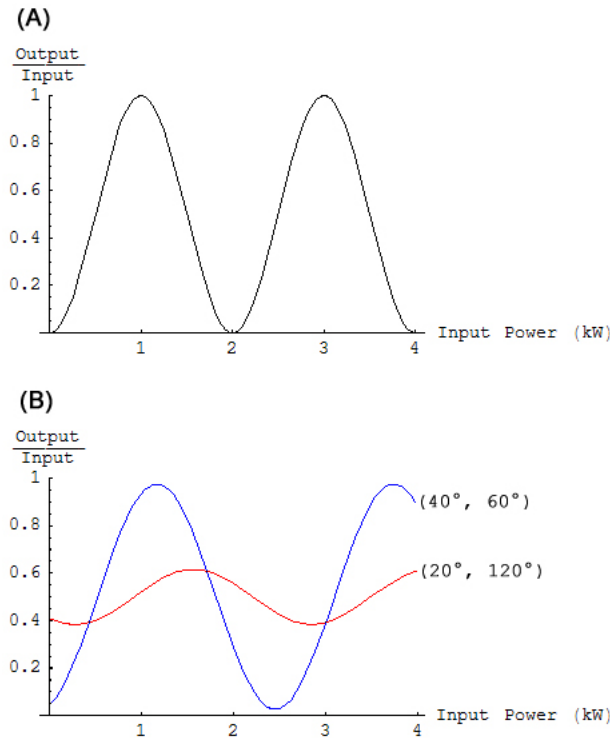


Figure 2.4 Example plots of power transfer through the NOLM. The horizontal axis displays the power of a light beam coupled into the NOLM input pigtail, the vertical axis shows the fractional power observed on the output pigtail. The PTC for our NOLM is always sinusoidal. **A.** PTC neglecting polarization in the NOLM. **B.** Example of two possible PTC's when polarization is included in the model.

Measurements of average laser power output indicate that the peak power of a pulse in the laser cavity is close to the vertical axis of the NOLM power transfer curve. Our current understanding is that modelocking only occurs when the PTC has a positive slope at low input powers (the laser's average cw power, near the vertical axis in Figure 2.4) and allows intermediate transmission at low input powers. Since NOLM PTC's are sinusoidal, an intermediate fractional transmission when the PTC depth of modulation is high indicates that the PTC slope is near maximum. It makes sense for the laser to modelock under these conditions because a positive PTC slope at low input power means

that the laser cavity discriminates against low intensity light, which creates an “incentive” for the laser to pack its energy into short pulses and maximize their transmission. A larger slope increases this discrimination and thus increases the likelihood of modelocking. Conversely, a negative PTC slope would discourage pulse formation because pulses, with high peak power compared to a cw beam, would be discriminated against instead.

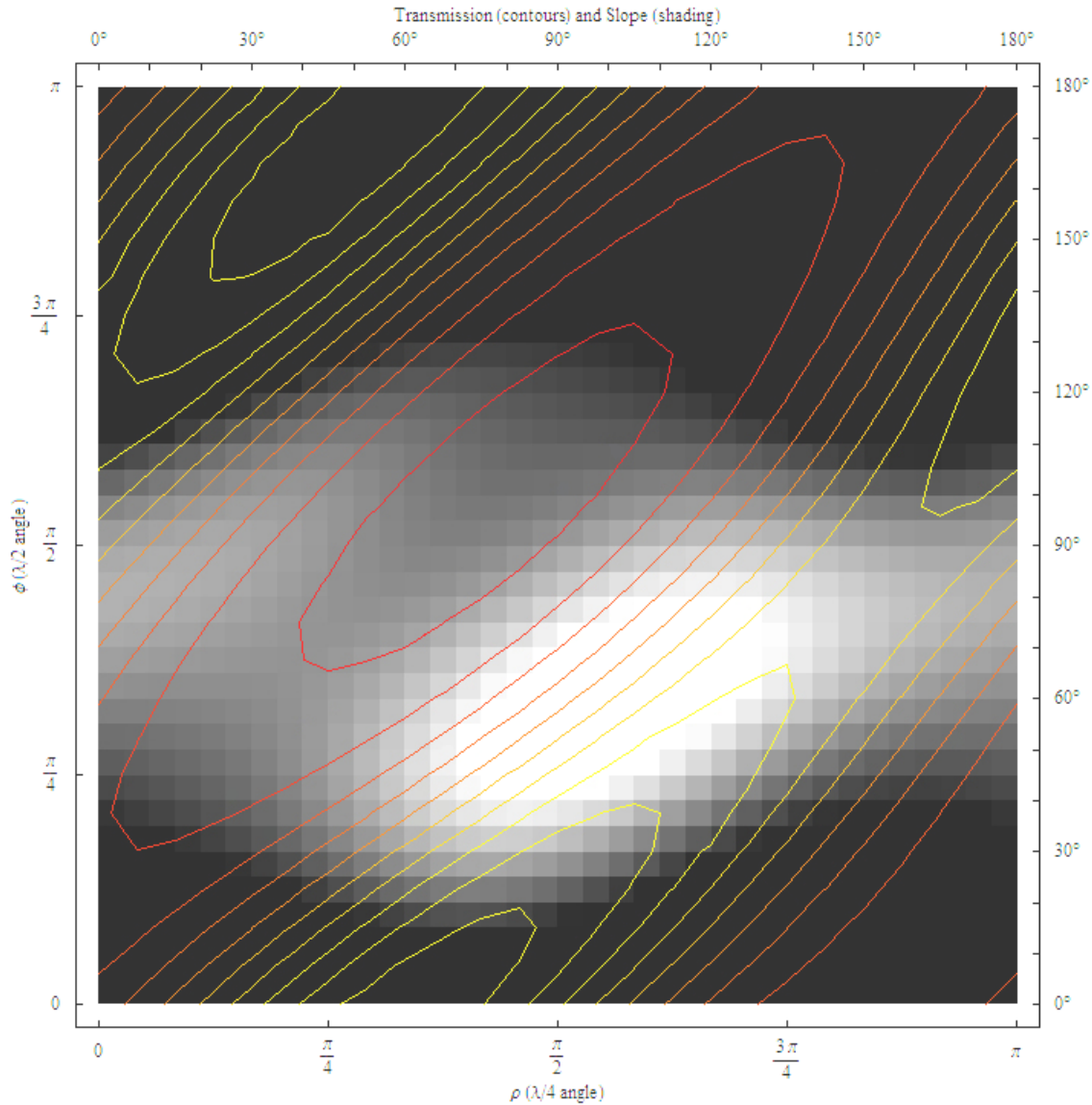


Figure 2.5 Polarization “map.” The axes mark the angles of the wave plates in the NOLM polarization controller; the horizontal axis is the quarter wave plate ρ and the vertical axis is the half wave plate ϕ . The low input power transmission through the NOLM (effectively the vertical intercept of the PTC) is shown as contour lines. Red contours signify low transmission, yellow contours signify high transmission. The bright shaded region encloses polarization settings at which the PTC slope is positive for low input powers (brighter shading means higher slope). A black background signifies negative PTC slope.

Power transfer curves can be calculated using the model developed by Murray in 2004-2005. Using the appropriate Jones matrices for each of the wave plates in the NOLM, the model is able to predict a power transfer curve for any given set of wave plate angles (ρ, φ). Figure 2.5 plots the critical information provided by this model. Each point on this figure corresponds to a polarization setting with a particular power transfer curve. The graph displays low-power fractional transmission through the NOLM, corresponding to the value of the power transfer curve near zero on the horizontal axis, as contour lines. Red contours represent low transmission while yellow contours indicate high transmission. White background shading distinguishes polarizations at which the PTC has a positive slope at low input powers. (Conversely, black shading marks polarizations with negative or zero low-input PTC slopes.) Since positive PTC slope can be viewed as an “incentive” for pulse formation, we expect the laser to be most likely to modelock at polarization settings where Figure 2.5 has the brightest shading (highest slope).

This model is fit to experimental data. The fiber in the NOLM must be bent in order to feasibly construct the loop, imparting bend-induced birefringence into the NOLM. We have dubbed this unknown phase delay the “mystery wave plate,” and we absorb it into the model with a Jones matrix for an arbitrary wave plate. Once the Jones matrices have been multiplied out, we can compute the polarization vector sum of the clockwise- and counterclockwise-propagating beams and determine the light intensity observed on the NOLM output pigtail, leaving the mystery wave plate phase delay and fast axis angle as variables. We then make measurements of low-power cw light transmission through the NOLM as a function of polarization controller wave plate angles. This data is used to seed the model: using the cw transmission data as the value of the PTC near zero input, we can have a computer find a numerical fit for the mystery wave plate phase delay and angle. Once we have the mystery wave plate parameters, we can use the Jones matrices to find power transfer curves at any polarization controller settings. All predictions using the NOLM polarization model rely on this low-power transmission data.

2.5 Diagnostic Measurements

Our lab is equipped to observe temporal pulse profiles from the fiber laser in two ways. Over long time scales—longer, that is, than the pulse width—we can use a germanium photodiode and measure its response on an oscilloscope. The photodiode is sensitive to infrared wavelengths including $1.55 \mu\text{m}$ and has a fast response rate of approximately 400 MHz when connected to the oscilloscope. This gives us a trace of laser output intensity versus time. A pulse train is readily apparent as a series of intensity spikes. More slowly varying intensity behavior of the laser is also evident. However, the response time of the photodiode and oscilloscope are not fast enough to resolve the duration of individual pulses.

In order to measure the duration of an individual pulse, we use an autocorrelator built in our lab to indirectly measure the pulse intensity profile.¹¹ The autocorrelator splits a pulse train into two beams, and we can introduce a time delay between these beams before recombining them in a nonlinear crystal. The crystal responds to the simultaneous absorption of two photons (one from each beam) by emitting a single

photon, a phenomenon called *second harmonic generation* (SHG), which is then detected. A plot of SHG intensity versus time delay is recorded. Mathematically, the x coordinate of an autocorrelation data point corresponds to the introduced time delay. The y coordinate is proportional to the value obtained by integrating the product of the delayed and un-delayed pulse profiles. Neglecting normalizing factors, an autocorrelation function can be expressed as

$$G(\tau) = \int_{-\infty}^{\infty} I(t)I(t + \tau)dt, \quad (2.7)$$

where I is the pulse intensity envelope and τ is the time delay.¹² The autocorrelation of a pure soliton will be a hyperbolic secant squared.

Another diagnostic measure we make in the laboratory is the transmission through the NOLM at low input powers. This can be determined with a low power 1.52 μm HeNe laser and an infrared-sensitive photodiode. We couple HeNe light into the unused pigtail on the WDM coupler (see Figure 2.2) which allows it to be injected directly through the Faraday isolator into the NOLM. Using the photodiode, we measure the transmitted intensity on the output coupler. As we record the NOLM throughput, we raster through quarter and half wave plate angles on the NOLM polarization controller to build up data on NOLM transmission over the full range of polarization settings. We take this low-power transmission data to be the value of the power transfer curve very close to zero input power and use it to find the phase delay and angle of the mystery wave plate through a numerical least-squares fit.

References

- ¹ Ferreira *et al.*, 2005
- ² Kivshar, Yuri S. and Govind P. Agrawal. *Optical Solitons*. Academic Press: San Diego, CA, 2003
- ³ Agrawal, Govind P. *Nonlinear Fiber Optics*. Academic Press: San Diego, CA, 1989
- ⁴ Ferreira *et al.*, 2005
- ⁵ Stievater, Todd. An erbium-ytterbium doped fiber laser. Thesis, Williams College, 19955
- ⁶ Ulrich, R., Rashleigh, S. C., and Eickhoff, W. Bending-induced birefringence in single-mode fibers. *Optics Letters* 5, 273-275 (1980)
- ⁷ Doran, N. J. and David Wood. Nonlinear-optical loop mirror. *Optics Letters* 13, 56-58 (1988)
- ⁸ Siegman, Anthony E. *Lasers*. University Science Books: Mill Valley, CA, 1986.
- ⁹ Kivshar and Agrawal, 2003
- ¹⁰ Murray, 2005
- ¹¹ Maginnis, Kira. Construction of a background free signal averaged autocorrelator. Thesis, Williams College, 1995
- ¹² Ippen, E. P. and C. V. Shank. Techniques for measurement. In *Ultrashort Light Pulses: Picosecond Techniques and Applications*; Schapiro, S. L., ed. Springer-Verlag: New York, 1977. p. 83-122

Chapter 3. Components of the Simulator

3.1 Optical Fibers

Simulations of solitons propagating in optical fibers are well documented in fiber communications literature.^{1, 2, 3} In general, any pulse in an optical fiber that has more energy than a first-order soliton should evolve into a soliton as it propagates. Based on this principle, all-fiber lasers with sufficient power should produce soliton pulses due to the action of shaping mechanisms in optical fibers. However, our all-fiber laser cavity contains other components that have significant pulse-shaping effects. We are interested in investigating the combined effect of all these components to determine how close our laser pulses are to solitons.

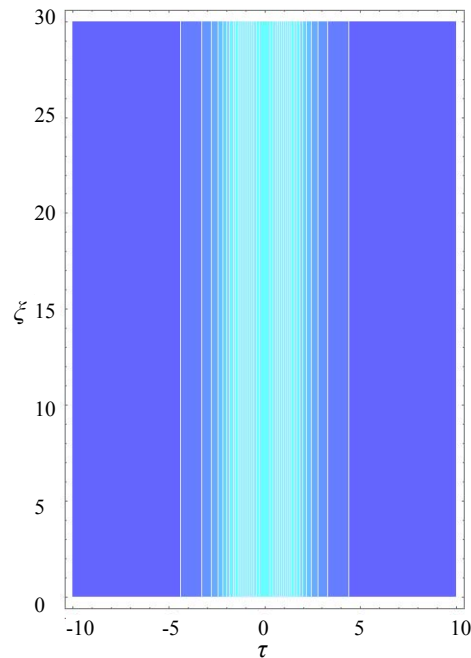


Figure 3.1 *Mathematica* simulation of a first-order soliton, $I = |\text{Sech}[\tau]|^2$, propagating in an optical fiber. This pulse shape remains unchanged as it propagates. Time delay from the pulse center is on the horizontal axis, distance of propagation is on the vertical axis, and contours display pulse intensity (all in dimensionless units). The pulse propagates upwards on this graph.

Optical fibers themselves have significant pulse-shaping effects. The nonlinear Schrödinger equation (NLSE) governs the propagation of pulses in optical fibers, as discussed in Chapter 2. The NLSE accounts for both dispersion and nonlinearity in fibers. Dispersion in the standard fiber of the laser cavity is the primary effect preventing the laser from producing delta-function pulses with infinitesimal width. The narrower a pulse is, the larger the bandwidth, and the more dispersion will cause the pulse to spread apart.

Given an input pulse shape at the beginning of a length of fiber, we can ask a computer to solve the NLSE and output the resulting envelope shape after the pulse has propagated some distance through the fiber. In *Mathematica*, this is done using the `NDSolve` routine with the input pulse given as a boundary condition at position $\zeta = 0$. `NDSolve` chooses from a number of explicit and implicit finite-difference methods with adaptive step sizes to solve partial differential equations.⁴ If the input pulse is a first-order soliton, the pulse shape will remain unchanged over any length of fiber (see Figure 3.1). If, however, the pulse has additional structure, more interesting behavior can result during propagation (Figure 3.2).

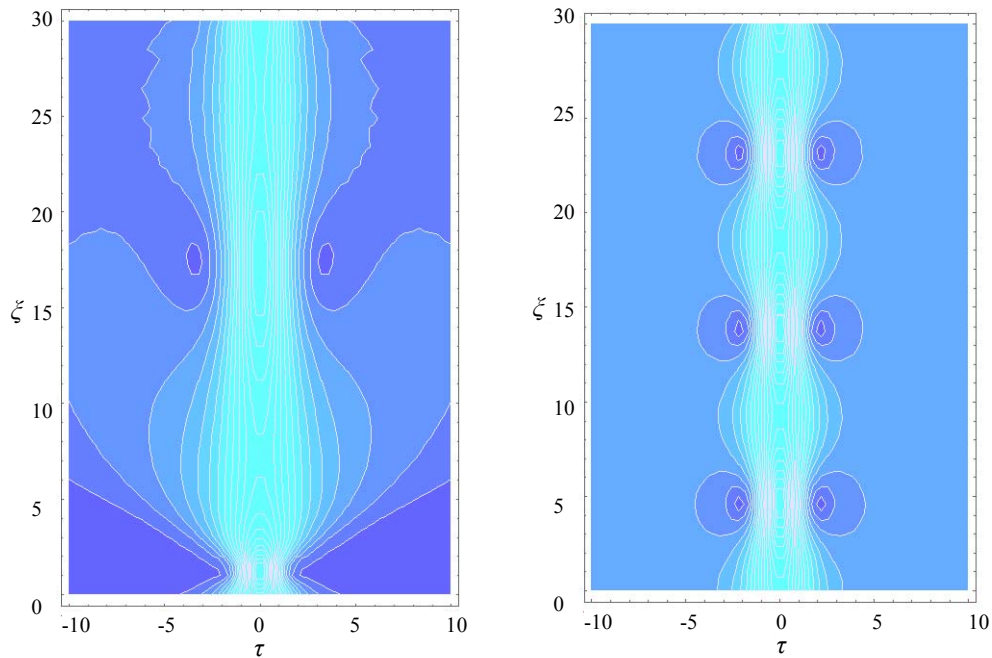


Figure 3.2 *Mathematica* simulation of solitons with additional structure propagating in an optical fiber. *Left:* A first-order soliton with a linear up-chirp across the pulse envelope, $I = |\text{Sech}[\tau] \text{Exp}[-i\tau^2/4]|^2$, develops complex “wing” structures that carry energy away from the pulse. *Right:* A first-order soliton with a constant additive background, $I = |0.8\text{Sech}[\tau] + 0.2|^2$, develops periodic “wings.”

The graphs in Figure 3.2 show that a soliton-like pulse can evolve into a complex temporal profile if it propagates far enough in a fiber. On the left is the result of inserting a soliton with a linear chirp into the NLSE. The pulse narrows slightly before exhibiting significant broadening. The broad “wings” of this pulse will, in fact, separate completely

from the central peak and carry energy away from the pulse. Though this numerical result begins to break down near the end of the simulation, other simulations have indicated that the pulse will eventually bleed off all extra energy from the chirp and evolve into a first-order soliton.⁵ Decreasing the maximum step size of `NDSolve` improves the resolution of the numerical solution at large ζ ; though the general behavior of the solution is independent of numerical step size until the distance of propagation is large enough for numerical errors to dominate the solution. Fortunately, there is not enough fiber in the laser to require a solution of the NLSE beyond a fraction of a unit in ζ . In fact, since we are interested in such relatively short distances, we can safely increase the maximum step size to save computation time. In contrast to a chirped pulse, a soliton with a constant background will not lose its extra energy. The right side of Figure 3.2 shows that such a pulse will exhibit strongly periodic behavior when injected into the NLSE. “Dips” form in the background offset and disappear again, returning the pulse to its original shape after some distance. The absence of numerical artifacts in this simulation suggests that this is a stable result of solving the NLSE, and the pulse should continue this periodic behavior over an indefinite length of fiber.

Mathematica works best in dimensionless units, where $\zeta = 1$ represents one dispersion length in the fiber, $\tau = 1$ represents one fundamental soliton width, and the peak intensity of a fundamental soliton is 1. The appropriate scaling factors for the nonlinear Schrödinger equation are given by Equation 2.4 and are listed in Table 3.1. The laser cavity contains lengths of standard optical fiber, dispersion shifted fiber, and erbium/ytterbium-doped fiber. Each of these may require its own scaling factors (currently, the Er/Yb fiber is taken to have identical characteristics to the standard fiber). For example, when a simulated pulse travels from one type of fiber to another, it must be multiplied by the ratio of intensity scales. Furthermore, some methods of modeling the NOLM require pulse intensity to be measured in real units. We must be careful to scale the `NDSolve` input pulse properly.

	Standard fiber	Dispersion-shifted fiber
t_0	1 ps	1 ps
l_d	43 m	860 m *
E_0	1.974 $\mu\text{W}/\text{m}^2$	21.146 $\mu\text{W}/\text{m}^2$

Table 3.1 Scaling parameters used in the simulation. t_0 is fixed, l_d and E_0 are calculated for a first-order soliton from t_0 , values for β_2 , n_2 , and other constants obtained from technical documentation on the Corning Optical Fiber web site, <www.corning.com/opticalfiber>. * The listed β_2 for DSF is an upper bound, so l_d for that fiber is a lower limit.

3.2 NOLM Pulse Shaping

There are several ways of modeling the nonlinear optical loop mirror in the fiber laser cavity. One conceptually satisfying method is to divide an input pulse into two unequal, counter-propagating pulses at the coupler, solve the NLSE for each pulse over the proper length of dispersion-shifted fiber, and add the pulse electric fields together again at the coupler. This approach has the intuitive advantage of closely mimicking the

physical behavior of the laser cavity; however, it is very computationally intensive and does not include polarization within the NOLM. An alternative method is to simply apply a pre-calculated power transfer curve to the input pulse, since the power transfer curve encapsulates all the behavior of the NOLM (refer to Section 2.4). At each point in time, the program multiplies the pulse intensity value by the appropriate fractional transmission factor given in the power transfer curve. Using a power transfer curve instead of the NLSE discards the effects of dispersion, but this is justifiable because the NOLM is composed of fiber with near-zero dispersion. Thus, we can replace two calls of `NDSolve` with a series of multiplications, saving computation power and time.

The NOLM is a lossy mechanism, so each trip through the NOLM should decrease pulse intensity. This energy must be replenished by the Er-doped fiber in order for laser pulses to remain viable in the laser cavity. In addition to decreasing pulse energy, we expect the nonlinear optical loop mirror to narrow pulses during each round trip of the cavity. We know that the laser should only modelock when the power transfer curve has a positive slope in the input power regime of our laser, close to the vertical axis. Due to this positive slope, the NOLM is *less* transparent to a lower input power than a higher input power. Within a pulse, the leading and trailing edges of the pulse envelope are less intense than the pulse peak; the pulse edges therefore experience lower fractional transmission than the peak. The net result is to narrow pulses. (By an analogous argument, a power transfer curve with *negative* slope should broaden pulses.) We have confirmed that applying a positively sloped power transfer curve in the model does indeed have this effect, illustrated in Figure 3.3. This figure shows the intensity profile of a single pulse that has passed through the NOLM the indicated number of times. After each passage, the pulse was rescaled to its initial peak height to prevent it from decaying away after a few round trips. We see that the NOLM indeed narrows pulses over many round trips. When a pulse in the laser cavity exits the NOLM, dispersion in the standard fibers will cause it to spread out again, preventing the loop mirror from narrowing any pulse to infinitesimal width. These simulations indicate that the competing effects of the nonlinear optical loop mirror and dispersion in the optical fibers must balance to produce pulses of a stable width.

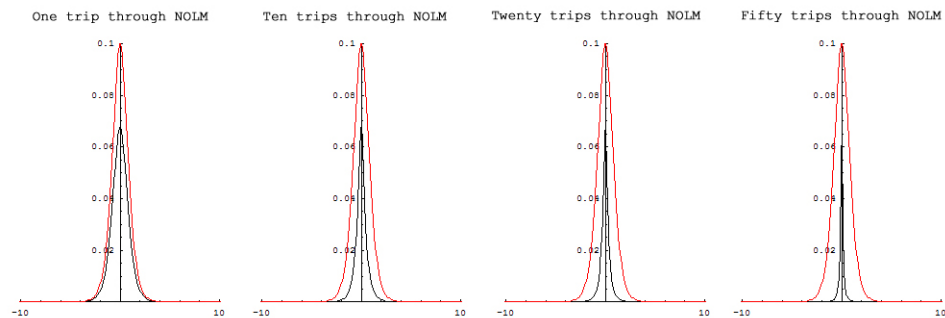


Figure 3.3 Example of how the NOLM, acting alone, narrows pulses over many round trips. No other components (fiber, gain) are present in the simulations. Plots show dimensionless intensity versus time delay for a single pulse after many trips through the NOLM. The red line represents the initial input pulse.

3.3 Laser Gain

The NOLM, Faraday isolator, output coupler, and splices are all lossy elements. Every round trip through the laser cavity, a pulse passes through a section of fiber doped with pumped erbium and ytterbium, regaining its lost energy via stimulated emission. We have attempted to simulate this process using a number of methods in the *Mathematica* program. These include renormalizing pulse profiles every round trip, multiplying pulses by a constant gain factor, and utilizing a variation of the nonlinear Schrödinger equation that takes linear gain into account. This portion of the simulator is not yet fully understood. Gain depletion and gain saturation, two processes that may have significant pulse shaping effects, have not yet been satisfactorily implemented in the model. Program output can be very sensitive to the gain simulation method chosen.

The simplest way to model laser gain is to multiply the pulse envelope by some gain factor. For example, pulses may be renormalized to the original input pulse energy. However, this method does not accurately reflect the physical system. Renormalization implies that *any* pulse injected into the laser cavity, no matter how large or small, will be replenished with the exact amount of energy that it started with each round trip. This should only be true in the steady state. The laser is brought into pulsed operation by introducing noise into the cavity; spikes of noise are shaped and amplified into modelocked pulses. We should therefore expect the model to be capable of building an arbitrary input pulse into a stable steady state with more energy than the initial pulse contained. A possible way to implement this capability is to multiply pulse envelopes by a fixed gain factor each round trip. Unfortunately, finding a value of the gain factor that causes pulses to reach and remain in a steady state, instead of decaying to zero or growing indefinitely, is a tedious and difficult process that we have not yet been able to automate.

Currently, we attempt to model the gain as rigorously as we can by using `NDSolve`. We can write the NLSE with a linear gain factor, g , on the right-hand side:

$$i \frac{\partial u}{\partial \xi} + \frac{1}{2} \frac{\partial^2 u}{\partial \tau^2} + |u|^2 u = gu . \quad (3.8)$$

This is, essentially, the Ginsburg-Landau equation with a number of parameters set to zero (we ignore such effects as nonlinear gain and spectral filtering).⁶ We have *Mathematica* solve this equation instead of Equation 2.3 to simulate pulse propagation through fiber doped with the gain medium. This method has the desired effect of increasing pulse energy and, for appropriate values of g , building up small seed pulses into steady-state pulses. Furthermore, using Equation 3.8 takes gain into account along the entire length of the Er/Yb-doped fiber rather than multiplying pulses by a gain factor that acts over an infinitesimal distance, which might not reflect the physical system as accurately.

We have programmed the simulator with an algorithm to determine g adaptively, since a value is not readily available. The model starts with an initial “guess” for g that is intentionally too small to permit lasing. The simulator repeatedly runs through a single round trip with a fresh seed pulse each time. The gain factor is doubled each iteration until the output pulse grows unstably, estimating an upper bound on g . The program

them halves g , and the simulation restarts with the injection of a new seed pulse. After each round trip, the program checks to see if the pulse peak has increased or decreased substantially and adjusts the gain factor by progressively smaller amounts to “home in” on a proper value. In a typical simulator run, the model settles on a value within five to ten cavity round trips. We implemented this adaptive algorithm for ease of computation, but it seems fairly robust. This final value of g does not depend greatly on seed pulse shape. Indeed, in most simulator runs, $g \approx 752 \pm 4$ whenever the simulator produces soliton-like pulses. Furthermore, the gain value obtained may be provided explicitly to the program, without the adaptive algorithm, and the simulator will produce identical steady-state results. Additional investigation is necessary to determine whether or not the gain parameter found by the program is reasonable.

In addition to increasing pulse energy, gain may affect pulse shapes in several ways. These include *gain saturation*, which causes the gain factor to depend on pulse intensity, and *gain depletion*, which causes the gain to depend on time. In the absence of both these effects, each photon in a pulse triggers stimulated emission from the gain medium with equal weight. A more realistic model of a gain medium includes a saturable gain factor, given by

$$g = \frac{g_0}{1 + I / I_{sat}}, \quad (3.9)$$

where I_{sat} is the saturation intensity of the gain medium.⁷ This would cause pulse edges to experience more relative amplification than the pulse peak, resulting in flatter pulses. We implemented a saturable gain factor into the program, solving Equation 3.8 to simulate laser gain, but found that the minimum value of I_{sat} that allowed pulsed lasing was much greater than typical pulse peak intensities. (In a typical simulator run, I / I_{sat} was on the order of 1/350 at the pulse peak, so that $g \approx g_0$.)

Gain depletion is the result of the population inversion being substantially exhausted before a pulse has completely traversed the gain medium. This results in the leading edge and peak of a pulse receiving more amplification than the trailing edge, changing the pulse shape considerably. g thus becomes a function of time delay τ . However, when using Equation 3.8 to model gain, *Mathematica* seems unable to handle a time-dependent gain factor. We may be able to implement gain depletion if a multiplicative constant can be used to simulate the Er-doped fiber. Alternatively, the model could be modified to use additional terms of the Ginsburg-Landau equation to simulate pulse response to nonlinear gain. These effects merit further study because of their potential pulse shaping abilities.

One more gain-related effect merits consideration in the model. Excited atoms in the gain medium can decay to the ground state through either stimulated emission or spontaneous emission. A population inversion in the gain medium implies that the probability of stimulated emission is much greater than the probability of spontaneous emission, so we have thus far neglected spontaneous emission in our discussion of laser operation. However, some of the erbium atoms may still emit 1.55 μm photons spontaneously. Other excited erbium atoms can amplify these extraneous photons in a process known as *amplified spontaneous emission*, or ASE.⁸ While ASE is occurring, we can expect to see pulse profiles that do not completely decay to zero for a long time

before or after the pulse center. Note that the presence of substantial gain depletion in the laser would preclude ASE. Amplified spontaneous emission has been implemented in the simulator in two alternative ways: after solving Equation 3.8, the program either adds a series of random noise values with random phases (with a specified maximum) to the electric field of the temporal pulse profile or it simply adds a constant offset to the profile. The former method sometimes produces different results on different simulation runs simply because we are introducing a random variable into the calculations. We interpret the latter option as either very low frequency ASE noise or a constant lasing background. The final results from each method do not exhibit substantial qualitative differences, though the exact correspondence between the parameters governing each method is not completely known. These parameters should reflect the ${}^4I_{15/2} \rightarrow {}^4I_{11/2}$ erbium excitation rate and ${}^4I_{13/2} \rightarrow {}^4I_{15/2}$ spontaneous decay rate.

3.4 Program Structure

We have programmed the *Mathematica* simulator to mimic the experimental apparatus, with some simplifications. As with many numerical simulations, the program attempts to strike a balance between accuracy and computational speed. Therefore, we have tried to make the simulator as simple as possible while still encapsulating all the pulse-shaping effects present in the fiber laser cavity. Like the laser itself, the model can be broken down into three major pieces: fiber, NOLM, and gain, as Figure 3.4 shows.

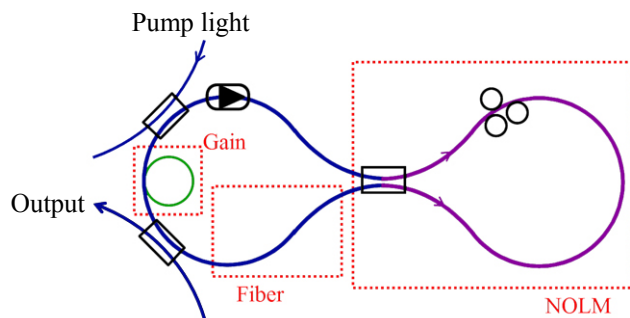


Figure 3.4 Diagram of the fiber laser cavity, with major pulse-shaping components highlighted.

Figure 3.5 provides a schematic illustration of the model after the adaptive gain algorithm has determined an initial upper bound on the gain parameter. Blocks represent chunks of *Mathematica* code, with the indicated inputs and outputs. The program begins by initializing a power transfer curve according to user-defined polarization controller settings, using the model developed in 2004-2005 (see Section 2.4). We also provide simulation runs with a seed pulse, most often a hyperbolic secant electric field envelope, which is injected into the simulator loop.

The model takes the seed pulse to be a pulse entering the gain medium, perhaps like the noise that initiates modelocking in the real system. It is given by a function of time delay and is linearly polarized, aligned with the Faraday isolator. The model begins by sending the pulse through 2 meters of gain fiber, solving Equation 3.8. The pulse traverses the nonlinear optical loop mirror next. The effect of the NOLM has been

collapsed into the pre-calculated power transfer curve, reducing the need for calculations within the simulator loop. Following the NOLM, the simulated pulse propagates through 13 meters of standard communications fiber by having the program solve the NLSE. At this point, the approximate location of the 10% output coupler in the physical system, the program stores the result in an array of pulse shapes as the output of the first cavity round trip. The program continues by checking the pulse peak, adjusting the gain parameter as necessary, and recycling the pulse into the gain medium. We assume it to have a linear polarization again after passing through the polarization controller and Faraday isolator. The simulator loop may be repeated any number of times, building up an output array showing the pulse shape after each round trip. In most simulator runs using parameters that produce modelocking, the pulse profile reaches a steady state after a reasonable number of round trips (typically ten to twenty when using the adaptive gain algorithm). Usually, the steady state pulse has much higher peak intensity than the seed pulse, an indication that seed pulse shape is not an important parameter in the simulator.

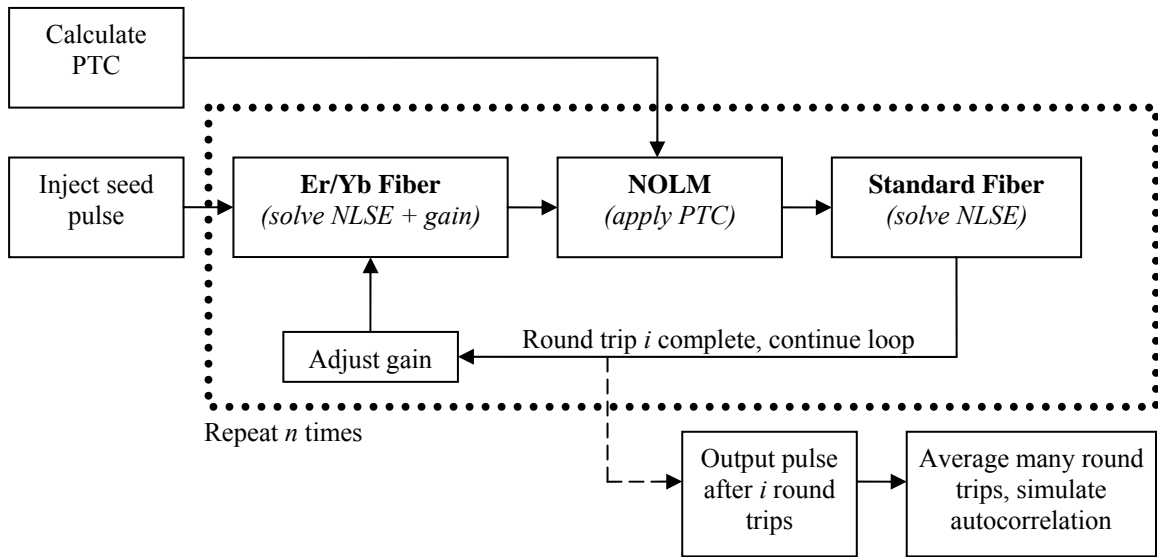


Figure 3.5 Block diagram of the *Mathematica* model used to simulate the fiber laser cavity shown in Figure 3.4. See text for full explanation.

The program can display simulator output in several ways. For example, we can access individual output pulses in the array after a particular number of round trips and display them as raw intensity profiles. The program is also capable of simulating an autocorrelation (our experimental method for indirectly measuring pulse profiles, discussed in Section 2.5) by multiplying a pulse profile by a time-delayed version of itself and integrating to produce a value proportional to the autocorrelation intensity for the given time delay. The program steps over a range of time delays to produce a simulated autocorrelation trace. To further mimic the experimental environment, in which the autocorrelator photodiode measures the time-averaged SHG intensity resulting from many pulses, the simulator can average many pulses together before computing the autocorrelation trace. Pulse intensities are averaged instead of autocorrelations (as in

experiments) purely for computational speed; the results should not differ if the simulated pulse shape has reached a steady state.

This model incorporates a number of simplifying assumptions about the laser. First, it does not explicitly take into account all the potential losses in the laser cavity. Besides the NOLM, these include fiber splices, the output and WDM couplers, and the Faraday isolator. We assume that the simulator implicitly includes these losses in the gain factor, which then represents a *net* gain. Second, we ignore dispersion in the NOLM. The 78m long loop is comprised of dispersion-shifted fiber that, at 1.55 μm wavelengths, has a dispersion parameter of only 0.9 ps km⁻¹ nm⁻¹, maximum, compared to 18 ps km⁻¹ nm⁻¹ in the standard fiber. Over one trip through the NOLM, a pulse acquires little complex structure as depicted in Figure 3.2, because the 78 m loop is small compared to the dispersion-shifted fiber's minimum dispersion length $l_d = 860$ m for a fundamental soliton (see Table 3.1). Furthermore, the amount of standard fiber in the cavity, when normalized to soliton dispersion lengths, is much greater than the normalized amount of dispersion-shifted fiber. We therefore take the effect of dispersion in the loop to be negligible, especially compared to the amount of pulse shaping that will occur in fiber outside the NOLM. This simplification allows us to apply a power transfer curve instead of solving the NLSE many times. Finally, the simulator lumps all the standard fiber in the laser into one section of the program. Figure 3.4 and Figure 3.5 illustrate this graphically: several meters of standard fiber make up the "pigtailed" between fiber optic components, but the simulator places all the standard fiber immediately after the NOLM. We make this assumption for ease of computation because 13 m of standard fiber (plus 2 m of Er/Yb-doped fiber) is less than SMF-28's characteristic length of 43 m. Thus, we expect fiber propagation effects to build up over many round trips of the laser cavity, rather than becoming significant during the course of a single round trip.

References

- ¹ Akhmediev, N., *et al.* Dissipative soliton interactions inside a fiber laser cavity. *Optical Fiber Technology* 11, 209-228 (2005)
- ² Desem, C., and P. L. Chu. Effect of chirping on solution propagation in single-mode optical fibers. *Optics Letters* 11, 248-250 (1986)
- ³ Tang, D. Y., L. M. Zhao, and B. Zhao. Soliton collapse and bunched noise-like pulse generation in a passively mode-locked fiber ring laser. *Optics Express* 13, 2289-2294 (2005)
- ⁴ Wolfram, Stephen. *The Mathematica Book*. Wolfram Media: Champaign, IL, 1996
- ⁵ Desem and Chu, 1986
- ⁶ Akhmediev *et al.*, 2005
- ⁷ Siegman, 1986
- ⁸ Siegman, 1986

Chapter 4. Results and Discussion

4.1 Experimental Results

We measure laser output using the methods described in Section 2.5. This fiber laser produces pulses about one picosecond or less in duration, approximately 420 nanoseconds apart. A typical oscilloscope trace of laser output measured on the germanium photodiode is shown in Figure 4.1. The trace duration is 1000 ns, clearly

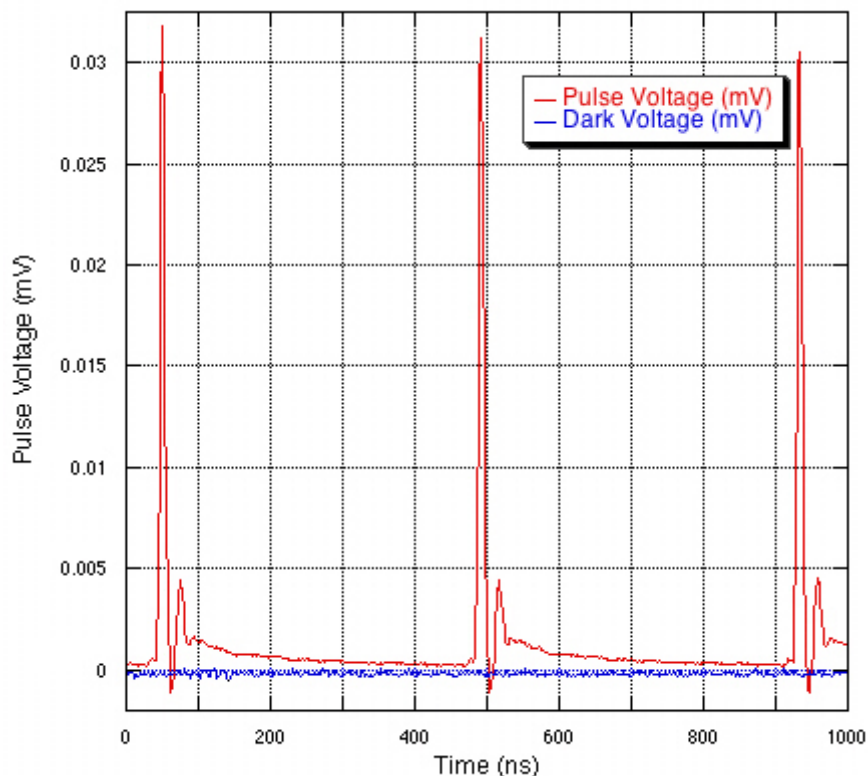


Figure 4.1 Oscilloscope trace of a modelocked pulse train emitted by the fiber laser. Note that the laser output remains above the dark level of the photodiode between pulses. The oscilloscope signals were averaged over several tens of seconds to reduce noise.

showing the 440 ns round-trip repetition time of the fiber laser. The intensity spikes correspond to ringing in the electronic system excited by the photodiode's impulse response to a very short optical pulse. These spikes are much longer (on the order of 10

ns) than measured autocorrelation widths (between 1.0 ps and 1.5 ps for modelocked pulses, see Figure 4.2). We also recorded the dark level of the photodiode by blocking the laser beam while the diode was active. Note that the pulse train does not decay to this dark level after the ringing has been damped. We infer from this observation that the fiber laser is actively lasing between pulses due to ASE. We observe background lasing on the oscilloscope immediately before each pulse, when ringing does not obscure the intensity trace. After a pulse, ringing in the electronics masks the trace, but ASE could be present in the laser at these times as long as the pulse has not depleted the population inversion enough to make spontaneous emission unlikely. If the population inversion is depleted by a pulse, it is sufficiently regenerated to produce spontaneous emission by 100 ns, maximum, after each pulse (this is approximately the time after a pulse when we can be sure the electronic ringing has been damped). However, as we shall see in Section 4.2, ASE is sufficient to explain autocorrelation backgrounds and non-soliton structure in pulse profiles, so we are confident that the ringing does not obscure a significant drop in background intensity. This implies that gain depletion may not be needed in the model. Additionally, we sometimes observe long-duration exponential decay of the laser output after a pulse on the oscilloscope, while at other times the background lasing seems constant; this remains unexplained.

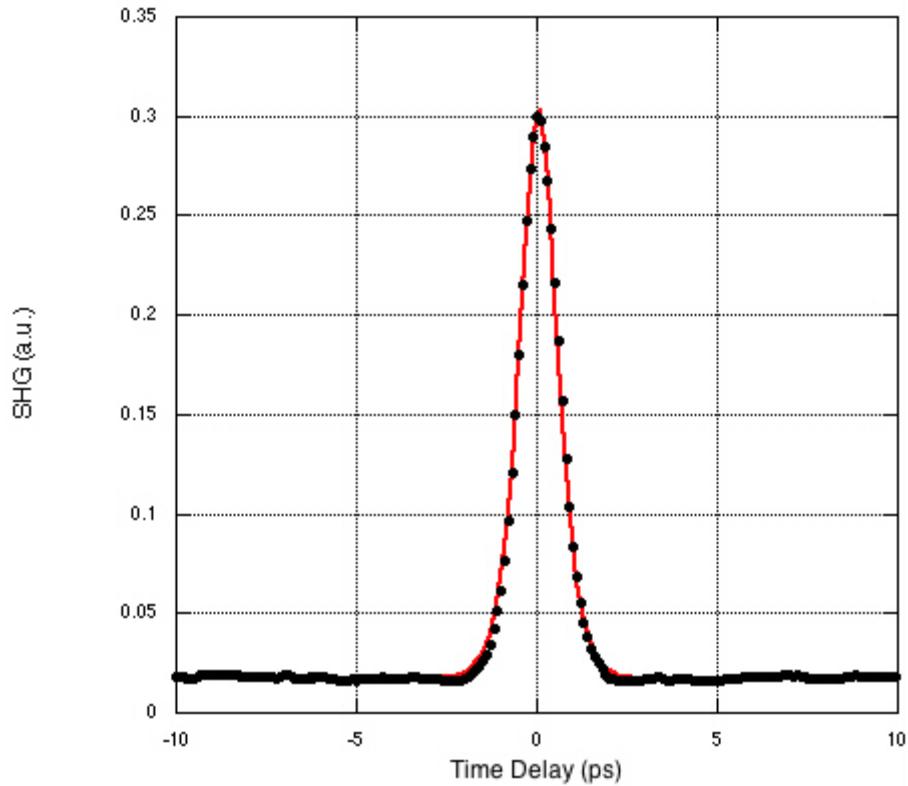


Figure 4.2 Autocorrelation of a typical laser pulse obtained at ($\rho = 71^\circ$, $\varphi = 65^\circ$). Time scale is in picoseconds, SHG intensity is in arbitrary units. The red line shows a fit to the expected hyperbolic secant squared. The full-width of this autocorrelation, obtained from the fit curve, is 1.39 ps.

When laser output is autocorrelated to reveal the structure of the pulses, we observe several different pulse shapes depending on the polarization settings within the NOLM. A typical experimentally obtained autocorrelation is shown in Figure 4.2. Figure 4.3 displays a number of autocorrelations representing the full range of pulse shapes we observe. These autocorrelations demonstrate that the pulses emitted by the fiber laser are not solitons, though the central peaks are usually a close match to a soliton shape. We interpret these autocorrelations to represent pulses that have a basic soliton shape.

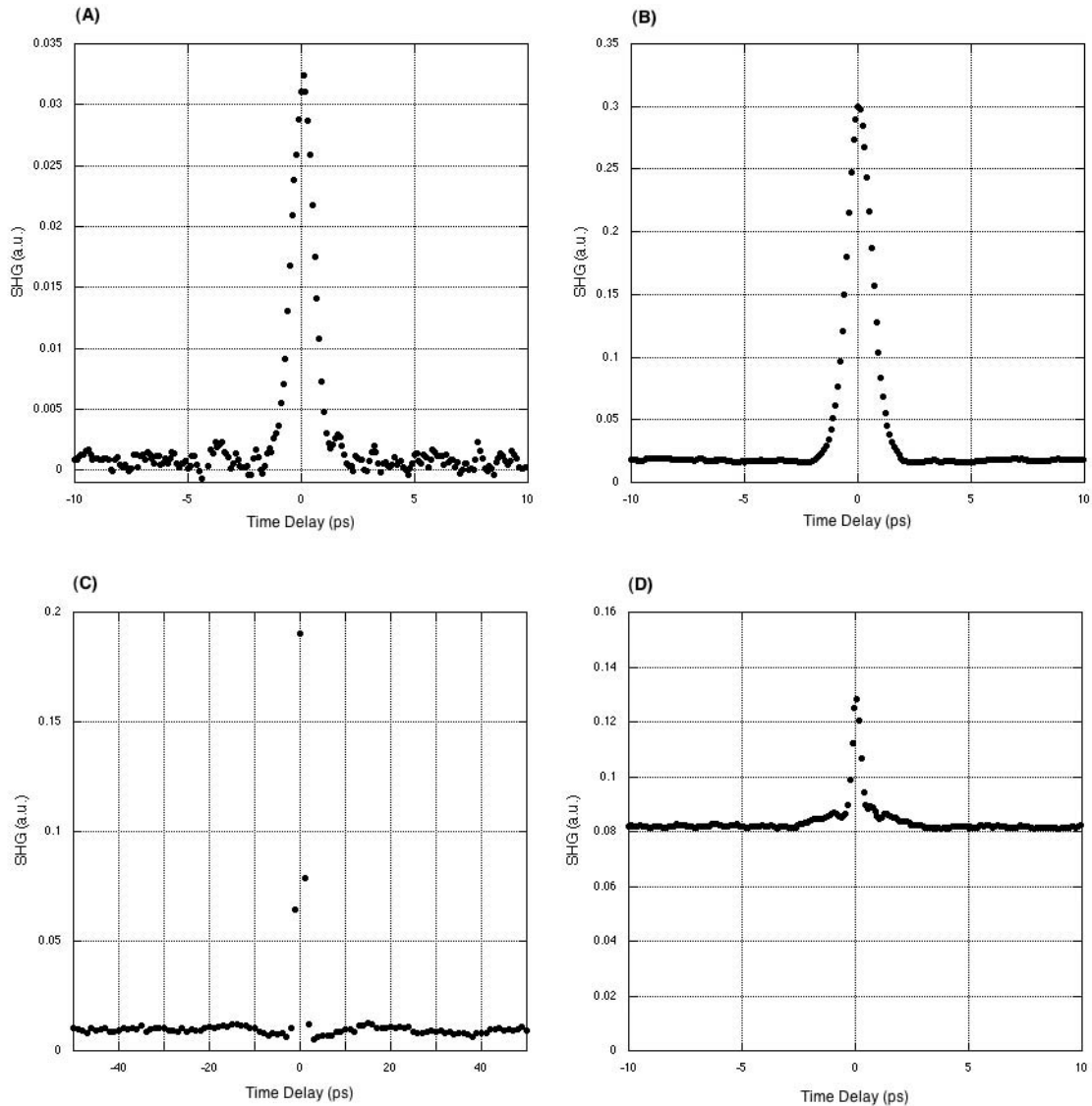


Figure 4.3 Experimentally recorded autocorrelations of a number of laser pulses, reflecting the wide range of output shapes observed at various polarization settings. A. A modelocked soliton-like pulse with a fairly low pedestal and no distinguishable wings or dips (note the low peak intensity compared to B-C, however). B. Soliton-like pulse with a pedestal of about 7% of the peak value. C. Pulse with dips (at about ± 3 ps) and wings (peaking at about ± 15 ps). The central peak is soliton-like, though not resolved well in this scan. D. Characteristic autocorrelation of a coherent noise spike. The peak intensity is not quite twice the background because the peak is not well resolved.

shape plus additional structure. We have developed nomenclature for those secondary structures that commonly appear in our measurements. We use the term *pedestal* to refer to a constant or slowly decaying offset (Figure 4.3B provides an example of an observed soliton with a pedestal). *Dip* refers to a decrease in autocorrelation intensity adjacent to the central pulse peak (see Figure 4.3C). Finally, the term *wing* refers to an increase in autocorrelation intensity at a temporal coordinate outside the dip, if present. Wings and dips are often paired as in Figure 4.3C.

We have also observed autocorrelations that do not correspond to modelocked pulses (Figure 4.3D). These autocorrelations consist of a very narrow central peak with a constant background of 50% of the peak value. This is the signature of a coherent *noise spike* or *noise burst*. In this situation, random noise in the laser cavity is responsible for laser pulsing, rather than modelocking. At a time delay of zero, the correlation function of the noise with itself is one, giving the central spike. At other time delays, an average of half the noise will produce SHG photons in the autocorrelator, thus the 50% background.¹ The oscilloscope trace of a noise burst is identical to that of a modelocked pulse, indicating that we are observing a transient burst of noise and the 50% background decays away between the range of the autocorrelator (about ± 150 ps) and the limit of resolution of the photodiode.

Oscilloscope traces such as Figure 4.1 show a background offset of approximately 10% of the spike peaks. To determine whether or not our oscilloscope backgrounds are consistent with the SHG intensity of autocorrelation pedestals, we employ a series of order-of-magnitude estimates. Since the laser pulse duration is shorter than the response time of the photodiode and oscilloscope, the oscilloscope does not have time to respond to the full peak intensity of a pulse before the pulse has passed. We expect the oscilloscope to record the total pulse energy, however, so the area under the recorded intensity curve and the true intensity curve should be the same. Using this fact, we relate the peak intensity on the scope to the full intensity by the ratio of the pulse width on the scope to the measured width in autocorrelations. Therefore, we expect that the scope should underestimate pulse peak intensities by an order of approximately $10 \text{ ns} / 1 \text{ ps} = 10^4$, giving us an estimated background intensity of 10^{-5} times the peak intensity. Common autocorrelations of pulses with pedestals have pedestal-to-peak ratios of 3% to 7%. To figure out the intensity background needed to generate such a pedestal, we look at the autocorrelation function $G(\tau)$ (Equation 2.7) of a soliton with intensity $I(t)$ and an additive constant background intensity b . Assuming that the background is due to random noise in the laser cavity that is not coherent with the pulse, we can add these intensities instead of adding their respective electric fields:

$$G(\tau) = \int_{-\infty}^{\infty} (I(t) + b)(I(t + \tau) + b) dt. \quad (4.10)$$

When the integrand is multiplied out, we obtain

$$G(\tau) = \int_{-\infty}^{\infty} I(t)I(t + \tau) dt + \int_{-\infty}^{\infty} b^2 dt + 2 \int_{-\infty}^{\infty} bI(t) dt. \quad (4.11)$$

The two cross terms, each containing a product of b and either $I(t)$ or $I(t + \tau)$, have been combined. This is reasonable since the integral under $I(t)$ remains the same whether the soliton is delayed or not. The terms in Equation 4.11 represent, in order, the autocorrelation of the soliton, the background, and a mix of the two. The final term can be visualized as an autocorrelation where the soliton is rastered across the background. Both the second and third terms contribute to the autocorrelation pedestal.

We take b to be constant (or very slowly varying) over the experimental autocorrelation range. This causes the middle term to blow up, but we assume that b may only be nonzero for a finite span of time. It makes sense to define the background of a single pulse as nonzero only for the interval between pulses, ~ 400 ns. Replacing the infinite limits of the second integral with this interval, the last two terms of Equation 4.11 give us

$$G_{pedestal} = (400 \text{ ns})b^2 + (4 \text{ ps} \cdot \text{W} / \text{m}^2)b \quad (4.12)$$

because the area under a hyperbolic secant squared with a width of 1 ps is $2 \text{ ps} \cdot \text{W} / \text{m}^2$. To produce an autocorrelation pedestal of 10% of the pulse peak, this expression tells us that the background intensity (as measured with the oscilloscope) must be on the order of 10^{-4} times the pulse peak intensity. Though not a perfect match for the observed background on the oscilloscope, this order of magnitude calculation illustrates how a very small intensity background could result in a significant autocorrelation pedestal. Therefore, we must consider the possibility that the fiber laser produces background lasing at approximately this level even during pulsed operation.

4.2 Simulator Results: Pulse Profiles

We can demonstrate that the *Mathematica* simulator described in Chapter 3 is capable of replicating a number of features of the experimental data. Simulation output at various NOLM polarization settings has included modelocked pulses closely matching autocorrelations of solitons and broad pulses that may correspond to noise spikes. In addition, the inclusion of ASE in the simulated laser gain allows the program to produce soliton-like pulses that feature pedestals, wings, and dips.

Figure 4.4 illustrates a typical simulator output pulse for polarization settings that we expect to produce modelocked pulses. The simulator started with a hyperbolic secant as the seed pulse, computed the resulting pulse shapes after each of 50 round trips through the laser cavity, then autocorrelated the average of the last 40 round trips. The simulator had achieved a steady state or near-steady state by the tenth round trip. Simulator output is shown in black. The red curve is a hyperbolic secant squared, the shape of a first-order soliton. Notice that the *Mathematica* program has produced a pulse with a shape very close to a soliton. In addition, the width of this autocorrelation compares favorably with experimentally obtained pulse widths. We can only obtain actual pulse widths from autocorrelation widths if the shape of the pulse envelope is known. With the simulator, we have the luxury of knowing exactly what pulse shape was autocorrelated, and it closely matches a hyperbolic secant squared. According to Ippen and Shank,² the ratio of the autocorrelation width to pulse width for a hyperbolic secant squared is 1.55. For simulated pulses, which are not quite solitons, we can calculate this

ratio to be 1.76. We can then use these ratios to calculate the widths of the pulses autocorrelated in Figure 4.2 (experimental data), assuming that the pulses match either a hyperbolic secant profile or simulated pulse profile. We compare these widths to the widths of simulated pulses and autocorrelations from Figure 4.4. We show pulse widths and autocorrelation widths in Table 4.1. Using the width ratio for fundamental solitons, the experimental pulse has a FWHM 50% wider than the simulation. Using the ratio obtained from the simulator, the experimental pulse is 31% wider than in simulations. Thus, the program is able to roughly reproduce experimental pulse widths.

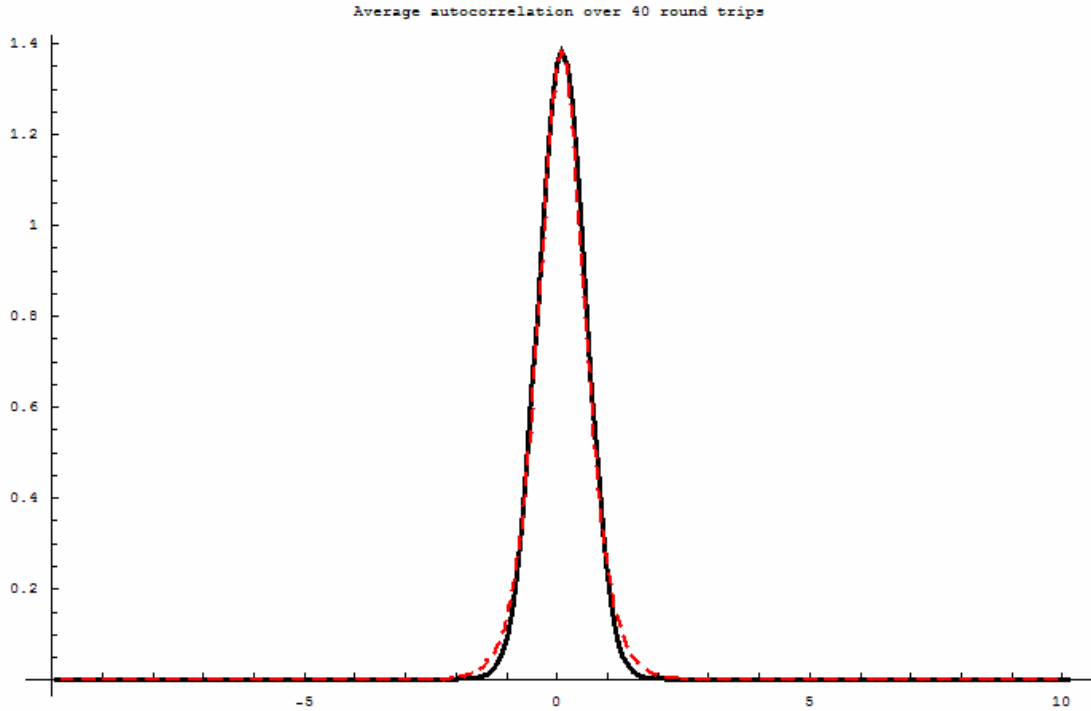


Figure 4.4 Simulated laser output at ($\rho = 64^\circ$, $\varphi = 43^\circ$), typical lab settings where modelocking is observed. Time scale is in picoseconds, intensity scale is SHG in arbitrary units. The black curve is the autocorrelation of the simulator output; the red, dashed curve is a hyperbolic secant squared. The simulator ran for 50 round trips and output was averaged over the last 40. The peak intensity of the seed pulse was 0.1 on this scale. Compare to data in Figure 4.2.

	Simulation	Experiment, using $\Delta\tau/\Delta t$ for soliton	Experiment, using $\Delta\tau/\Delta t$ from simulation
$\Delta\tau$	1.06 ps	1.39 ps	1.39 ps
Δt	0.600 ps	0.898 ps	0.786 ps

Table 4.1 Autocorrelation and source pulse widths for experimental data and computer simulations. *Simulation* refers to the results of Figure 4.4; *Experiment* refers to the data for Figure 4.2. $\Delta\tau$ is the full width at half max (FWHM) of the autocorrelation. Δt is the FWHM of the intensity profile that was autocorrelated. The second column assumes a soliton pulse shape, and $\Delta\tau/\Delta t = 1.55$. The last column uses $\Delta\tau/\Delta t = 1.76$, from the simulated widths in the first column.

The simulation pulse width was found to remain fairly constant in all simulator runs that produced modelocked pulses. Recall that t_0 is an arbitrary, mutable parameter, so we may be able to improve the agreement between simulations and experiment with further work. Initial investigations of the parameter t_0 indicate that changing it too much will cause the simulation to break down. The nearly constant pulse widths in simulations and the limitations on t_0 suggest that the fiber laser has a characteristic pulse width of less than a picosecond.

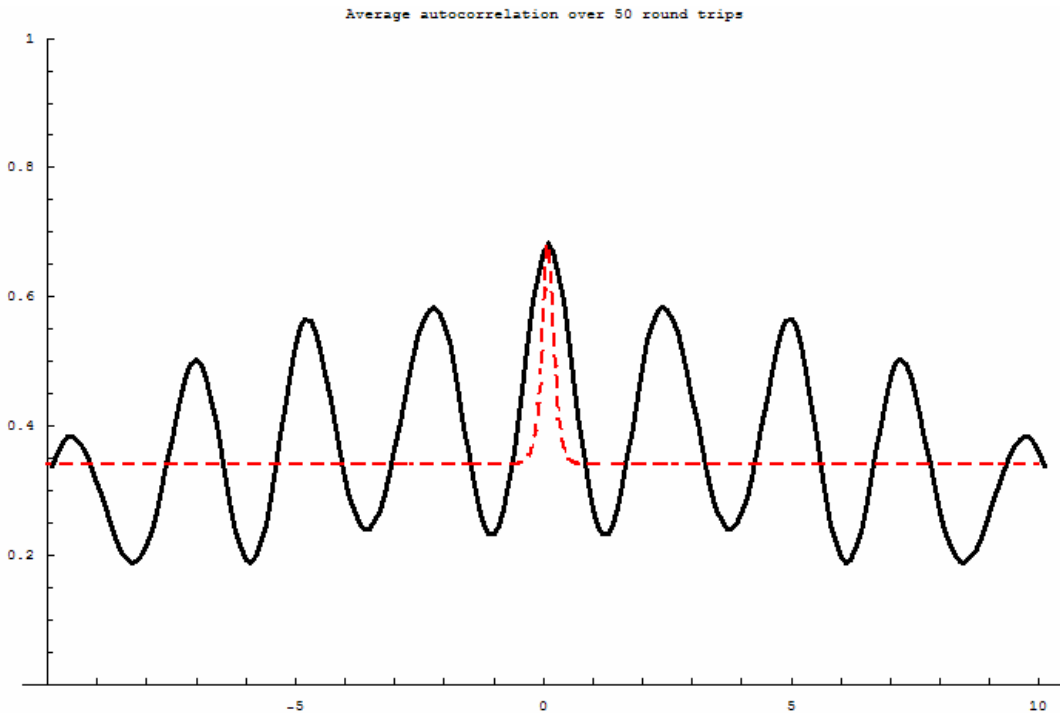


Figure 4.5 Simulated laser output at ($\rho = 80^\circ$, $\varphi = 180^\circ$), near one set of polarizations that has produced noise spikes in the lab. Time scale is in picoseconds, intensity scale is SHG in arbitrary units. The black curve is the autocorrelation of the simulator output; the red, dashed curve sketches an approximation of a noise spike. The simulator ran for 100 round trips and output was averaged over the last 50. The peak intensity of the seed pulse was 0.1 on this scale. Compare to data in Figure 4.2D.

When the simulator is run at polarization settings that correspond to negative power transfer curve slope, a much broader, more complex output pulse results (Figure 4.5). The simulated autocorrelation consists of a high central peak with additional structure oscillating about some nonzero SHG intensity around or above half the central peak intensity. These pulses do not reach a steady state within the first few tens of round trips as the modelocked pulses do; instead, they evolve a new set of oscillatory peaks every ten or twelve round trips. If the oscillations in these pulses were smeared temporally, they might average to a value of approximately half the central peak intensity, approximating the temporal profile of a noise spike. Though this simulator profile does not precisely correspond to experimental autocorrelations (see, for example, Figure 4.3D), this could conceivably be the signature the *Mathematica* program produces for noise spikes.

A more likely explanation of these output pulses is that they are simulation artifacts. They only occur at polarizations with negative PTC slope, where pulses should broaden and suffer a decrease in peak intensity. Given that the adaptive gain algorithm tests the pulse peak rather than the total pulse energy, it may be possible that the simulator is choosing a gain parameter high enough to boost the central portion of the pulse to a power past the first PTC minimum, where slope is positive again (refer to the examples of sinusoidal power transfer curves in Section 2.3). On subsequent passes through the NOLM in this case, the pulse could experience low transmission for an intermediate range of intensities but higher transmission for both low and high intensities, causing a triple-peak structure to develop from a single peak. Repeating this cycle of excess gain, broadening, and peak generation can account for the buildup of oscillatory structure in these simulated pulses. We might be able to avoid these artifacts in the future by reprogramming the adaptive gain algorithm to test whether or not the total energy (found by integration) in a pulse has increased or decreased substantially since the last round trip, rather than testing the pulse peak intensity. As of this writing, running the simulator with such a modification to the adaptive gain results in these artifacts becoming generally broader and lower in amplitude. Taking a simulation run with a very large number of round trips, much greater than the standard fifty or one hundred, may result in these pulses being broadened and weakened out of existence.

Pedestals, wings, and dips cannot be simulated simply by choosing the proper NOLM polarization settings. Instead, a new effect must be added to the simulator. We have found that adding a term to our model of the gain medium—Equation 3.8—to simulate amplified spontaneous emission causes the simulator to reproduce all three pulse structures (refer to Section 3.3 for a full discussion about simulating the laser gain). Figure 4.6 shows two resulting pulses, using two different methods to simulate ASE. Note that the near-soliton shape is preserved, but the autocorrelation does not quite reach zero at large time delays. This example shows pedestals of approximately (A) 1.5% and (B) 0.9% of the autocorrelation peak. These simulated pedestal amplitudes are smaller than those we observe in the experimental system. This could be due to the particular polarization settings chosen. Alternatively, it could be because the simulator only calculates the pedestal out to a 20 ps range, while in the experimental system, the pedestal may extend much further beyond the range of the autocorrelation. In effect, the simulator underestimates the contribution of the b^2 term in Equation 4.11 by using integration limits much smaller than a 400 ns range. There is not a substantial difference between the two ASE simulation methods in terms of qualitative pulse structure aside from the smoothness of the autocorrelation pedestal. The variations seen in Figure 4.6A are probably due to the randomness of the ASE simulation method chosen. These simulator results clearly indicate that the program is capable of reproducing an autocorrelation pedestal (shown in Figure 4.2 and Figure 4.3), the most frequently recorded variation from pure soliton pulses, with the inclusion of amplified stimulated emission.

We observe wings and dips at other polarization settings and ASE levels. A good example is provided in Figure 4.7. These wings, however, are seen much closer to the central peak than the experimentally recorded wings of Figure 4.3C. These simulated wings are consistent with some experimental results, and other simulations show wings at larger time delays. Note that even in the presence of secondary structure, the central peak

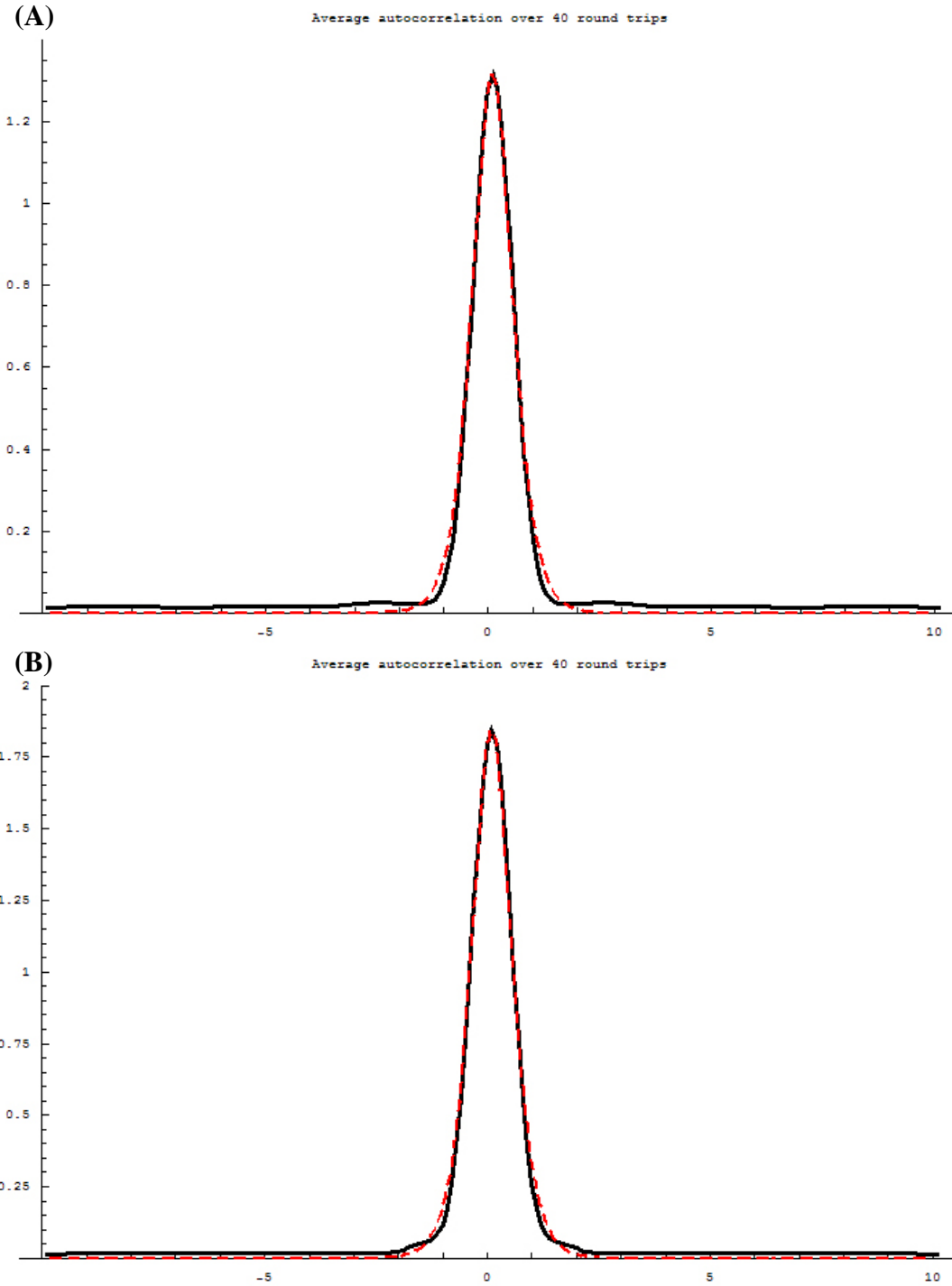


Figure 4.6 Simulated laser output at ($\rho = 140^\circ$, $\varphi = 60^\circ$), near lab settings where modelocking is observed, with ASE. Time scale is in picoseconds, intensity scale is SHG in arbitrary units. The black curve is the autocorrelation of the simulator output; the red, dashed curve is a hyperbolic secant squared. The simulator ran for 50 round trips and output was averaged over the last 40. The peak intensity of the seed pulse was 0.1 on this scale. Compare to data in Figure 4.2 and simulations in Figure 4.4. **A.** ASE added as random noise with maximum amplitude 0.016. **B.** ASE added as constant offset of magnitude 0.016.

remains at approximately the same width as in the other simulations shown in this section. The formation of dips from an ASE background can be easily understood through inspection of Figure 3.2. As depicted on the right of Figure 3.2, a soliton with a constant background will, when launched into an optical fiber, develop a periodic alternation between a background with dips and a constant background as it propagates along a fiber. This is simply the mathematical result of solving the NLSE with an input pulse that includes some ASE. The simulated pulses travel through over a third of a dispersion length of standard fiber, which may be enough for these wings (which are most pronounced after a distance of about five dispersion lengths) to begin developing. Once the pulse background has a slight dip, the narrowing action of the NOLM should apply to both the central pulse and the outer edges of the dips, accentuating them. Wings probably form through a similar mathematical mechanism in the NLSE. The ability of the simulator to duplicate observed secondary pulse structure coupled with our observations of background lasing between pulses suggests that amplified spontaneous emission is a good candidate explanation for the observed pedestal, wings, and dips.

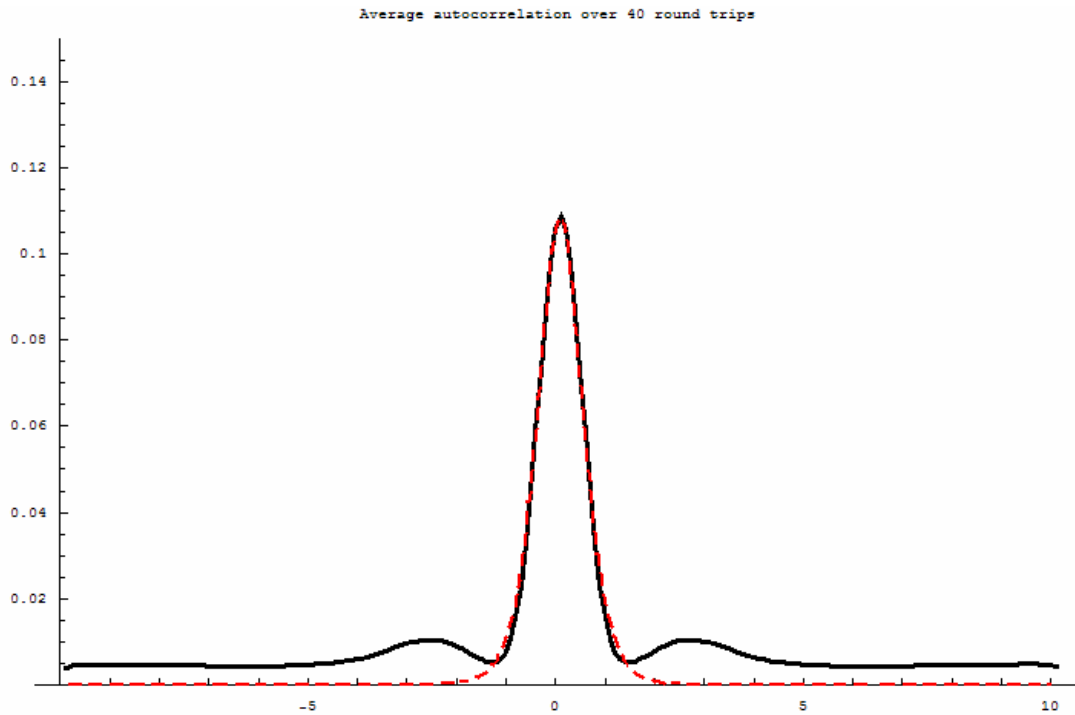


Figure 4.7 Simulated laser output at ($\rho = 120^\circ$, $\varphi = 35^\circ$), near lab settings where modelocking is observed, with ASE. Time scale is in picoseconds, intensity scale is SHG in arbitrary units. The black curve is the autocorrelation of the simulator output; the red, dashed curve is a hyperbolic secant squared. The simulator ran for 50 round trips and output was averaged over the last 40. The peak intensity of the seed pulse was 0.1 on this scale and ASE was added as random noise with maximum amplitude 0.009. Compare to experimental wings in Figure 4.3C.

4.3 Simulator Results: Polarization-Dependent Trends

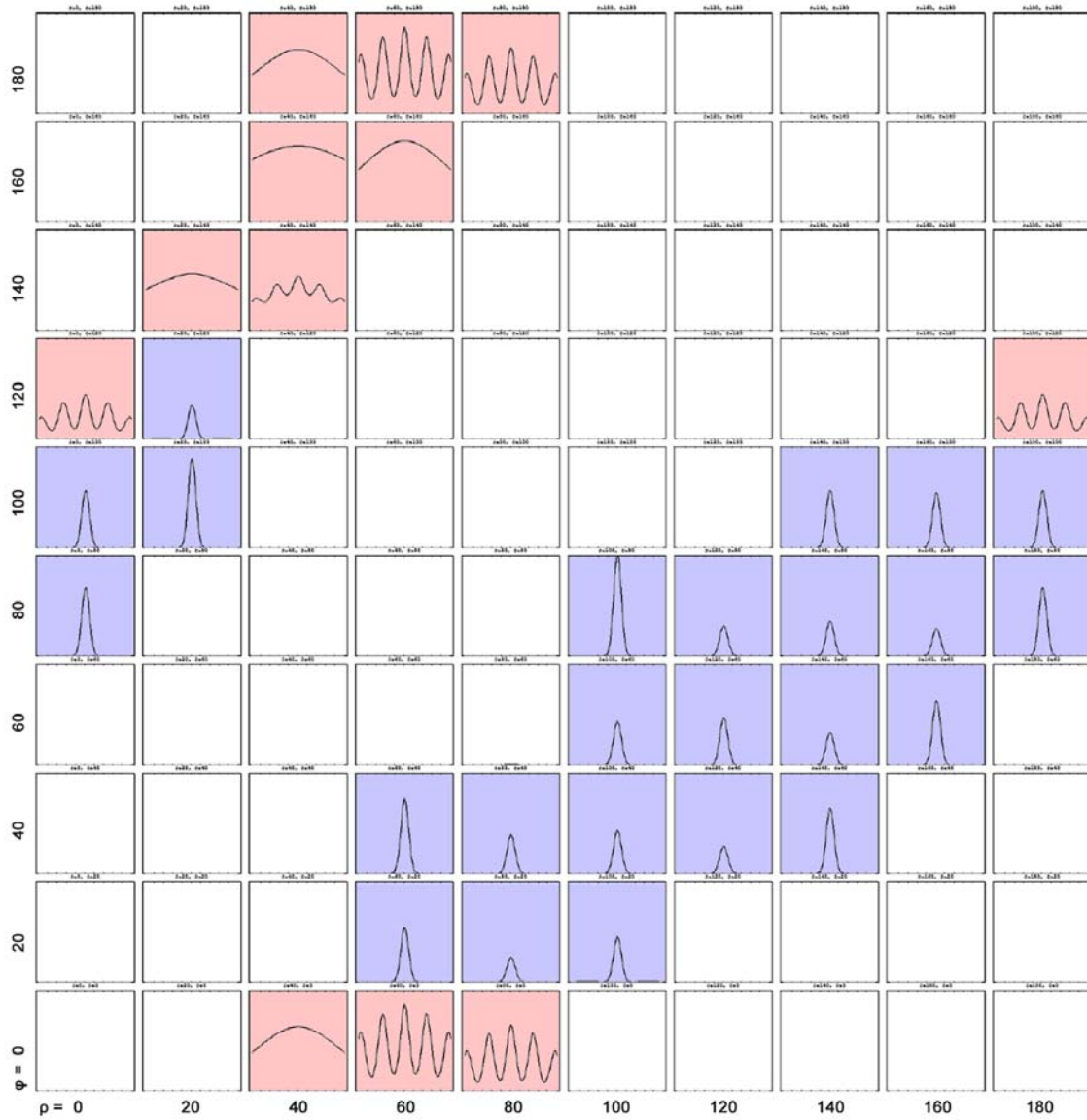


Figure 4.8 Autocorrelations of simulated pulse shapes for many NOLM polarizations without ASE. Output plots have been set up to correspond to the quarter and half wave plate angle axes as in Figure 2.5; quarter wave plate angle ρ runs horizontally and half wave plate angle φ runs vertically in steps of 20° . All plots are on temporal scales ranging to ± 5 ps, and all plots are on the same intensity scale in arbitrary units. Blue shading indicates a modelocked pulse; red shading indicates anything else (possibly a noise spike). This graph repeats in both wave plate dimensions with a period of 180° .

We have observed that the major variable determining the whether or not the fiber laser modelocks is the polarization of light within the NOLM. Any given set of polarization settings (combinations of quarter wave plate angle ρ and half wave plate angle φ) may allow the formation of modelocked pulses, coherent noise spikes, or

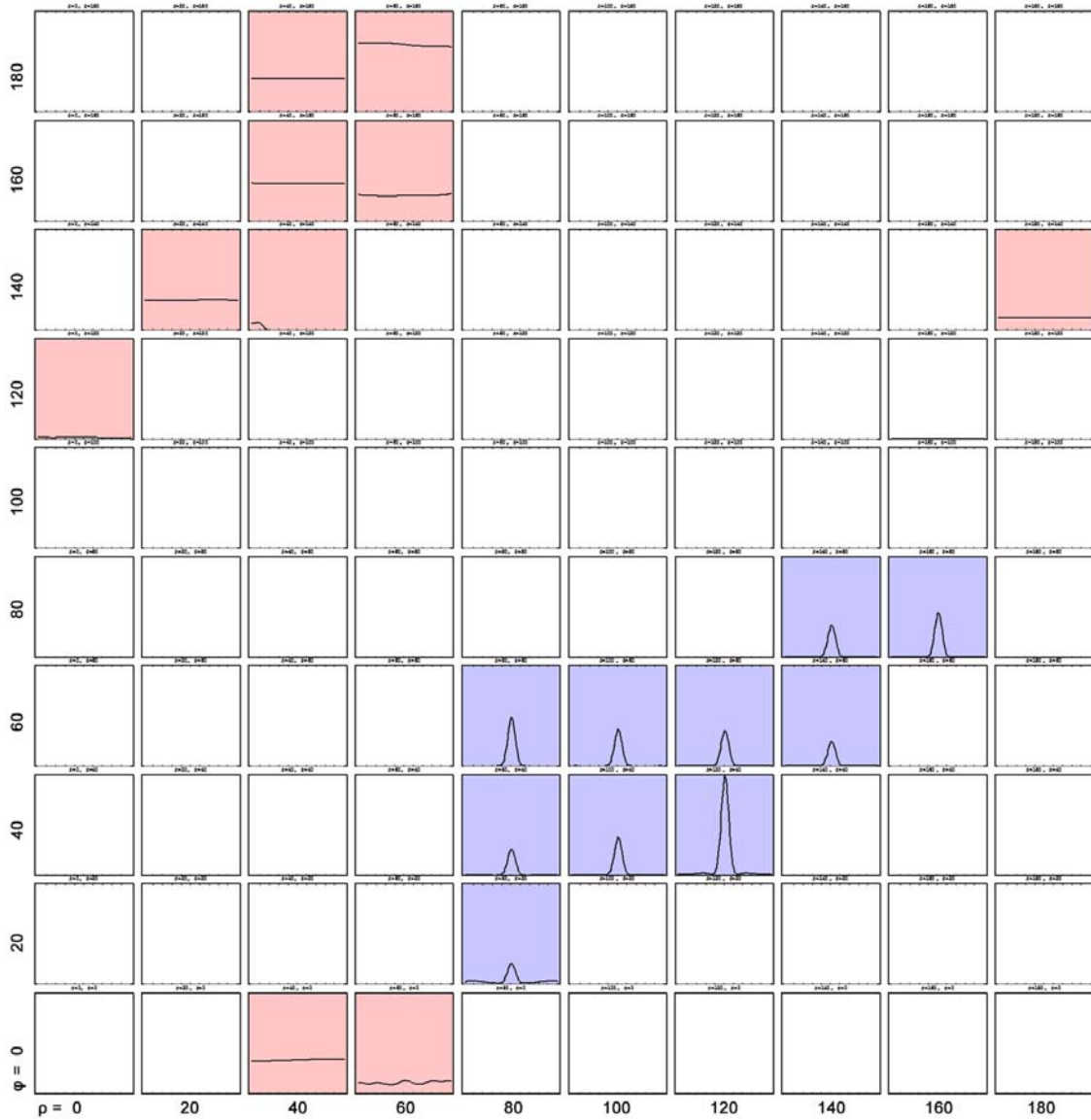


Figure 4.9 Autocorrelations of simulated pulse shapes for many NOLM polarizations with ASE included as random noise with maximum amplitude 0.016. Output plots have been set up to correspond to the quarter and half wave plate angle axes as in Figure 2.5; quarter wave plate angle ρ runs horizontally and half wave plate angle ϕ runs vertically in steps of 20° . All plots are on temporal scales ranging to ± 5 ps, and all plots are on the same intensity scale in arbitrary units. Blue shading indicates a modelocked pulse; red shading indicates anything else (possibly a noise spike). This graph repeats in both wave plate dimensions with a period of 180° .

neither. If modelocked pulses are allowed, wings and dips may be present. A pedestal is present on modelocked pulses in almost all cases. The *Mathematica* simulator is based on the model developed last year to identify polarization settings where modelocking is allowed and uses power transfer curves calculated from experimental data (Section 2.4).

We expect, therefore, that a robust simulator should mimic the dependence of the fiber laser on NOLM polarization settings.

A compilation of simulator runs, without ASE, at many different polarization settings is shown in Figure 4.8. All results shown in this figure are on the same time and intensity scales. The figure illustrates three major zones in our two-dimensional polarization space, roughly defined by this 20° -interval grid. Output pulse plots with blue shading correspond to modelocked pulses (note the nearly constant pulse width). Red shading indicates any pulse autocorrelation that does not match a modelocked pulse profile, possibly corresponding to noise spikes. Twice as many tested polarization settings produce modelocking as produce non-modelocked pulses. Finally, unshaded plots occur in “dead” spaces where simulated pulses either died away after a number of round trips or developed fatal numerical errors during a round trip of the laser cavity. At these polarization settings, the simulator predicts that no output pulses are possible.

A corresponding set of simulations including an arbitrary amount of amplified spontaneous emission as random additive noise produced Figure 4.9. There are fewer pulse-producing polarization settings indicated on the figure, and the ratio of polarization settings that produce non-modelocked pulses to polarization settings that encourage modelocked pulses has doubled to 1:1. Furthermore, all the modelocked pulses have a nonzero pedestal. Wings are evident in several of the simulated autocorrelations, particularly those at the $(120^\circ, 40^\circ)$ and $(80^\circ, 20^\circ)$ grid points. In fact, the simulated pulse at $(80^\circ, 20^\circ)$ has wings that peak at a time delay about 5 ps removed from the central soliton-like pulse. These wings are more distant from the pulse peak than those shown in Figure 4.7, illustrating that the simulator can produce a range of output profiles with the background structures we are looking for.

We are particularly interested in how the regions defined by modelocking behavior correspond to regions of high NOLM transmission or large power transfer curve slope. Using the polarization “map” of Figure 2.5 as a framework, the results of simulations can be compared to our model for NOLM behavior. Figure 4.10 displays a composite plot of simulated (X’s and shading) and experimental (dots) pulse behavior in the context of our polarization map. Blue dots represent polarizations at which modelocked pulses have been observed, while red dots show polarization settings at which the laser produces noise spikes. Likewise, blue X’s mark polarization settings of simulated modelocking and red X’s mark polarizations where non-modelocked pulses have been simulated.

Two important points must be kept in mind when referring to this graph: First, the simulated points are on a 20° mesh corresponding to the wave plate angles indicated in Figure 4.8. Each simulated pulse is marked explicitly by an X on the polarization map, but these points have been expanded into 20° by 20° shaded regions to indicate the overall area in which the simulation can support pulses. The areas suggested by the simulations are only approximations; these simulation runs are important for their overall behavior. Second, the absence of an experimental dot at a polarization setting does not necessarily mean that that polarization setting will not support pulses in the experimental system; rather, the absence of a dot merely indicates that pulses have not yet been observed at that point on the map. Similarly, the cluster of modelocked pulses around $(65^\circ, 40^\circ)$ does not necessarily imply that modelocking is statistically more likely at those polarizations. A systematic study of the NOLM polarizations that can and cannot

produce pulses in the fiber laser has not yet been performed, partly due to the fact that once the polarization controller in the NOLM has been set to a desired (ρ, φ) point, all three wave plates of the polarization controller preceding the Faraday isolator must be optimized (see Section 2.3).

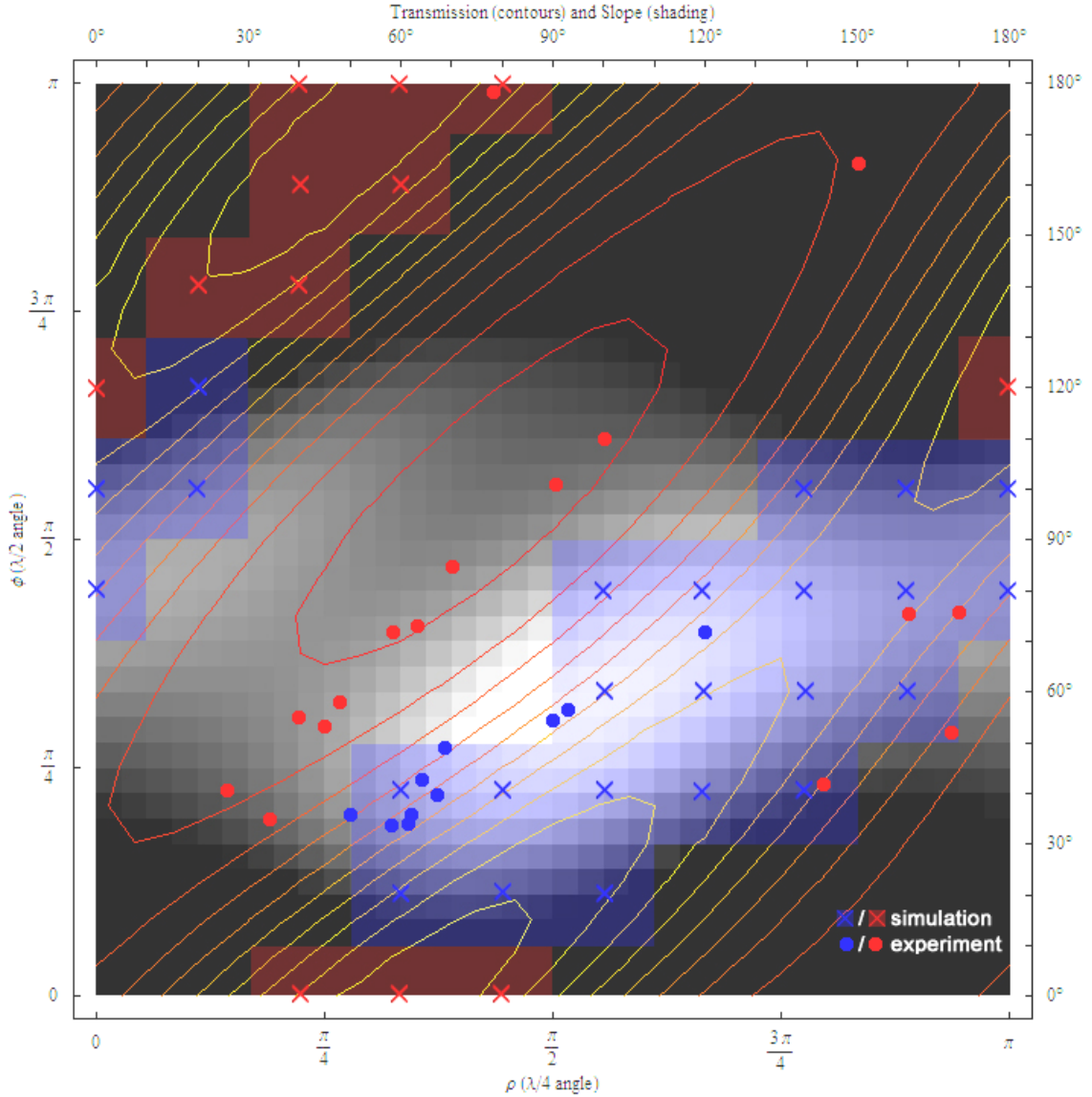


Figure 4.10 Compilation of experimental data, the model from Figure 2.5, and the simulations of Figure 4.8 (no ASE). The model for NOLM transmission (contours) and PTC slope (greyscale shading) is the same as Figure 2.5: yellow contours are higher transmission than red, white shading is positive PTC slope. Blue dots indicate polarizations where modelocking has been observed and red dots indicate polarizations where noise spikes have been observed in the lab. Blue X's mark the polarizations of modelocked pulses in Figure 4.8 and red X's mark polarizations of simulated non-modelocked pulses; shading indicates the approximate areas supporting each kind of pulse in simulations. This graph repeats in both wave plate dimensions with a period of 180° .

We can make a number of observations about this polarization map. A particularly encouraging point is that the simulator generates modelocked pulses exclusively at polarization settings where PTC slope is positive. This is consistent with experimental pulses obtained shortly after the polarization map in Figure 2.5 was produced. Notice that all the experimental modelocked points in Figure 4.10 fall within the region defined by the simulated modelocked points. In addition, there seems to be a roughly defined transmission minimum required to simulate pulses. We see this most clearly from the positions of the X's marking simulation points: judging from this map, no polarization settings on the simulated grid produce pulses if the NOLM transmission is much lower than about 25% of maximum. A transmission minimum is also consistent with experimental data, which suggests that approximately 30% transmission is preferable for modelocking.

However, the behavior of non-modelocked pulses in the model and the experiment do not match. While we have observed some noise spikes in the lab at polarizations where we expect negative PTC slope (as the simulator indicates we should), only one experimentally observed noise spike—near $(80^\circ, 180^\circ)$ —falls within the region of potential noise spikes defined by the simulator (assuming the non-modelocked pulses such as that in Figure 4.5 indeed represent simulated noise spikes). Many observed noise spikes were found at polarization settings falling in the “dead” zone suggested by the simulator in Figure 4.8. The *Mathematica* program seems to produce noise spikes at any polarization setting where NOLM low-power transmission is large enough. (The transmission minimum required by simulator noise spikes is higher than that required by simulator modelocking, allowing these pulses in a much smaller range of polarizations.) This mismatch supports the possibility that the oddly shaped pulses produced by the simulator at negative PTC slope are, in fact, simulation artifacts rather than the simulator's signature for noise spikes. Since the model does not allow pulses at those polarization settings where we have observed noise spikes in the lab, the mechanisms driving the formation of coherent noise spikes are apparently not supported by the simulator at this time.

Some correlations and inconsistencies between simulation and experiment in Figure 4.10 cannot be confirmed without more data. Careful study of the simulated pulses on this map indicates that the transmission minimum, rather than a PTC slope minimum, serves as the boundary of the pulsing region (for example, the simulator exhibits modelocking at both $(100^\circ, 60^\circ)$, a point with near-maximum slope, and $(20^\circ, 120^\circ)$, a point with very low—near zero—slope; while no point indicating modelocking falls much beneath the third transmission contour). The relative importance of PTC slope and transmission is not experimentally known. However, we expect positive slope to be very important, and the highest slope occurs at intermediate transmission.

Additionally, modelocked pulses have not been observed in the lab at polarization settings allowing NOLM transmission beyond a certain maximum, while the simulator supports modelocking at very high transmission as long as there is a positive PTC slope (for instance, $(80^\circ, 20^\circ)$ on the map). Comparison of the polarization-dependent trends shown in Figure 4.10 with the varying pulse shapes illustrated in Figure 4.8 suggests the possibility that pulse peak amplitude might be influenced by the NOLM transmission. Perhaps the experimental system cannot produce modelocked pulses when the pulse peak would be below a certain threshold. However, the correlation between simulated pulse

peak and NOLM transmission is not strong, though the simulated pulses with highest peaks occur at polarization settings near the settings where we most commonly observe modelocking in the lab. Finally, the simulator predicts modelocking at some polarizations with $\rho \leq 20^\circ$ and potential noise spikes in several regions where experimental data is not present to confirm these predictions. More detailed investigations of the pulsing behavior of the fiber laser must be carried out to validate the simulator.

References

¹ Ippen and Shank, 1977

² Ippen and Shank, 1977

Chapter 5. Conclusion

Until recently, we relied on the model proposed by Doran and Wood to explain the operation of the NOLM in our fiber laser. This model neglects the effect of polarization in the optical fiber comprising the NOLM. We realized that the polarization of light in the NOLM is an important factor in causing the laser to modelock. After a study of polarizations at which modelocking was observed, Aubryn Murray used Jones matrices to develop a model of NOLM behavior that includes the effect of polarization and is capable of predicting NOLM power transfer curves and, therefore, which polarization settings will allow modelocking. This model has become a standard tool in our lab.

However, a number of questions remained after Murray's work, centering on experimentally observed pulse shapes. We expected that pulses formed in an optical fiber cavity would be close to first-order solitons, but autocorrelations show that the laser produces soliton-like pulses with various background structures (pedestals, dips, and wings) or noise spikes. We did not have the understanding of optical pulse shaping mechanisms inside the laser cavity necessary to explain these observations.

Over the past year, we have developed a *Mathematica*-based numerical simulator to provide us with the ability to examine pulse-shaping mechanisms in the laser cavity and observe their effects on output pulses. This simulator explicitly accounts for the three major pulse-shaping mechanisms in the fiber laser: the soliton shaping effects of dispersion and self-phase modulation in the SMF-28 communications fiber, the pulse narrowing effect of the NOLM, and contributions to pulse shape from the gain medium (possibly including effects such as gain saturation, gain depletion, and amplified spontaneous emission). In simulating the nonlinear optical loop mirror, this *Mathematica* code integrates the polarization model developed last year. When simulating the effects of optical fibers or the gain medium, the program utilizes the nonlinear Schrödinger equation, which is used to investigate the propagation of solitons in optical fibers.

This simulator has confirmed a number of our suspicions and proven capable of reproducing several experimental results. First, output pulses from the simulator closely match the temporal profile of a first-order soliton, reinforcing the initial theory that the laser should produce soliton-like pulses. Second, the behavior of the simulator over the "polarization space" defined by the quarter and half wave plates in the NOLM suggests a match to experimental observations of pulses as a function of wave plate angle. This simulator result supports the NOLM polarization model developed last year and suggests that, with further refinement and an accurate low-power NOLM transmission map, the simulator could be used to predict polarization settings at which the fiber laser should modelock. Third, the inclusion of amplified stimulated emission in the simulations allows the program to produce output with background structures that mimic all those

that have been seen in autocorrelations and mystified us until this point. In fact, using the simulator to support our argument, we can state that a relatively small ASE background in the laser output can be held responsible for the autocorrelation pedestals we observe when the laser modelocks.

The development of the simulator has aided and solidified our understanding of the various pulse-shaping mechanisms present in the fiber laser cavity. We tested the propagation of several different pulse shapes through an optical fiber, demonstrating that the simulator can use the nonlinear Schrödinger equation to model optical fibers. Comparison of the scaling parameters used for standard communications fiber and dispersion shifted fiber led us to the conclusion that fiber pulse-shaping mechanisms can be neglected in the NOLM loop, allowing us to simplify and optimize the model. Furthermore, propagating pulses with a constant background through an optical fiber in numerical simulations has demonstrated that soliton shaping mechanisms can explain the wings and dips observed in autocorrelations.

Our conceptual picture of the nonlinear optical loop mirror has also improved as a result of work on the simulator. We can use the simulator to confirm that the NOLM does not just encourage pulse formation by passive modelocking; there are also definite pulse shaping effects from the loop mirror. In particular, when polarization settings are such that the power transfer curve slope is positive at low power, the NOLM will narrow a pulse. Combining the action of the NOLM with soliton shaping mechanisms in fibers indicates that the pulses produced by the fiber laser are not only the result of a balance between dispersion and self-phase modulation, as solitons are, but a balance between dispersion, SPM, and the narrowing effect of the NOLM.

Some open questions remain regarding the gain medium. Thus far, the simulator can demonstrate that amplified spontaneous emission, simulated in either of two ways, is viable in the laser cavity and is responsible for autocorrelation pedestals, wings, and dips. However, we have not yet determined the precise correspondence between the amount of simulated ASE and the pulse background structure. Before the simulator is used to make specific predictions about experimental pulse shapes, we will need to know the relationship between polarization settings, ASE parameters, and the shape and size of pedestals, wings, and dips. In addition, the effects of gain saturation and gain depletion could be further quantified and investigated. These effects may significantly change the shape of a pulse in the laser cavity but have been neglected in the most recent version of the simulator for the reasons given in Section 3.3. Further research could clarify these effects and indicate the accuracy of the current implementation of laser gain.

Now that we have developed a simulation framework, we can use pulse-shape simulations as another tool to investigate the fiber laser behavior. The effects of many parameters that are difficult to probe in the experimental system can be investigated. These could include the amount of dispersion in the laser cavity, the lengths of fiber used, the treatment of laser gain, or the addition of other components that would require invasive work on the experimental system. The simulator has already helped us to better understand pulse shaping inside the laser cavity. Some refinements to and features of the *Mathematica* program remain to be implemented in the future. It is hoped that as the simulator is improved it will become a standard tool in the lab, to be used alongside the experimental system. This simulator has already increased our ability to characterize the fiber laser a great deal. Using our acquired understanding of the laser, future work in our

lab can begin to focus on using the fiber laser as a test bed for investigating the propagation of soliton (or near-soliton) pulses in optical fibers.

Appendix

On the following pages is the *Mathematica* code for the simulator including amplified spontaneous emission. The program begins by initializing variables, including physical constants, fiber characteristics, and options such as the input pulse shape, number of round trips, or amount of ASE. The program then sets up the power transfer model of the NOLM as developed last year. Next, the adaptive gain algorithm runs a single round trip of the laser cavity several times, adjusting the gain parameter of the NLSE as necessary. Once a gain parameter is secured, the program begins its main loop, consisting of the gain fiber, the NOLM, and the standard communications fiber in turn. The loop can be run any number of times. After the program has completed, various snippets of code following the main block allow results to be displayed in any number of ways. On average, fifty round trips through the laser cavity take approximately three to five minutes to run on a reasonably fast computer.

Several variations of this code exist. Some include ASE, while others do not; some include various other effects such as gain saturation or gain depletion. Another useful variation runs the entire simulator inside a large loop. This can be used to cycle through many different settings on a single parameter or pair of parameters. That version was used to produce Figure 4.8 and Figure 4.9 by looping over the wave plate angles. The simulator sessions that produced those figures took approximately four to five hours to run.

Specific comments on the code can be found within the *Mathematica* program, contained in (* parentheses and asterisks*).

```
(* This program simulates an initial soliton pulse
   making multiple round-trips of the laser cavity.
```

```
    Important note: Sometimes, for reasons I can't fathom,
the program won't run until you change
the number of round trips to simulate. *)
```

```
Clear[ξ, τ, u, ρ, φ, gain, lastGain, gainPwr];
```

(* OPTIONS *)

```
(* Number of round trips to make *)
```

```
roundtrips = 50;
```

```
(* Input pulse shape *)
```

```
inputpulse = 1.0 Sech[τ];
```

```
(* Really, a first-order soliton is all that makes sense here *)
```

```
T = 1(*ps*) (10^-12); (* Width of input soliton *)
```

```
(* Waveplate angles *)
```

```
ρ = 64 (π/180);
```

```
φ = 43 (π/180);
```

```
(* Enter fit parameters from HeNe model here,
   or run HeNeAnalyzer and comment this line out *)
```

```
fitparms =
```

```
{δ → 3.3714258, f → 2.787589, ε → -0.85759979, x → -3.8771295};
```

```
(* Max steps to take in
```

```
   NDSolve. Mathematica default is 10,000. *)
```

```
steps = 100;
```

```
(* Fiber parameters *)
```

```
gainoffset = 0; (* pedestal gain *)
```

```
gainPwr = 2; (* Starting guess for gain (gain = 2^gainPwr)...
```

```
   program will alter this. this value is a lower bound,
```

```
   the program will increase it till it's appropriate. *)
```

```
α = .513;
```

```
n = 3.2;
```

```
Dsmf = 18(*ps/km nm*) (10^-12 / (10^3 10^-9));
```

```
Ddsf = 0.9(*ps/km nm*) (10^-12 / (10^3 10^-9));
```

```
λ = 1560(*nm*) (10^-9);
```

```
c = 3*^8(*m/s*);
```

```

ε0 = 8.85*^-12;

βsmf = λ^2 Dsmf / (2 π c);
βdsf = λ^2 Ddsf / (2 π c);

LDsmf = T^2 / βsmf (*m*);
LDdsf = T^2 / βdsf (*m*);

core = 3.0 (*microns*) 10^-6; (*fiber core radius*)
coreArea = π (core)^2;

n2 = 4.5*^-16 10^-4 (*10*^-22*);
ωzero = 2 π c / λ;

NOLMlength = 71.0 (*m*);
SMFlength = 13.0 (*m*);
Erlength = 2.0 (*m*);

NOLMphaseCW = i 2 π α n2 NOLMlength / λ;
NOLMphaseCCW = i 2 π (1 - α) n2 NOLMlength / λ;

qsmf = Sqrt[.5 n2 ωzero LDsmf / c];
qdsf = Sqrt[.5 n2 ωzero LDdsf / c];
qscale = qsmf / qdsf;

```

(* CALCULATE PTC *)

```

quartercw :=
  {{Exp[i * (π / 2 + ε) / 2] * (Cos[ρ - x])^2 + Exp[-i * (π / 2 + ε) / 2] *
    (Sin[ρ - x])^2, 2 i * Sin[(π / 2 + ε) / 2] * Cos[ρ - x] * Sin[ρ - x]},
  {2 i * Sin[(π / 2 + ε) / 2] * Cos[ρ - x] * Sin[ρ - x],
  Exp[-i * (π / 2 + ε) / 2] * (Cos[ρ - x])^2 +
  Exp[i * (π / 2 + ε) / 2] * (Sin[ρ - x])^2}}
halfcw := {{Exp[i * (π + 2 ε) / 2] * (Cos[φ - x])^2 +
  Exp[-i * (π + 2 ε) / 2] * (Sin[φ - x])^2,
  2 i * Sin[(π + 2 ε) / 2] * Cos[φ - x] * Sin[φ - x]},
  {2 i * Sin[(π + 2 ε) / 2] * Cos[φ - x] * Sin[φ - x],
  Exp[-i * (π + 2 ε) / 2] * (Cos[φ - x])^2 +
  Exp[i * (π + 2 ε) / 2] * (Sin[φ - x])^2}}
fibercw := {{Exp[i * δ / 2] * (Cos[f])^2 + Exp[-i * δ / 2] * (Sin[f])^2,
  2 i * Sin[δ / 2] * Cos[f] * Sin[f]}, {2 i * Sin[δ / 2] * Cos[f] * Sin[f],
  Exp[-i * δ / 2] * (Cos[f])^2 + Exp[i * δ / 2] * (Sin[f])^2}}
ccwfiber := {{Exp[i * δ / 2] * (Cos[π - f])^2 + Exp[-i * δ / 2] *
  (Sin[π - f])^2, 2 i * Sin[δ / 2] * Cos[π - f] * Sin[π - f]},
  {2 i * Sin[δ / 2] * Cos[π - f] * Sin[π - f],
  Exp[-i * δ / 2] * (Cos[π - f])^2 + Exp[i * δ / 2] * (Sin[π - f])^2}}
ccwhalf := {{Exp[i * (π + 2 ε) / 2] * (Cos[π - φ + x])^2 +
  Exp[-i * (π + 2 ε) / 2] * (Sin[π - φ + x])^2,
  2 i * Sin[(π + 2 ε) / 2] * Cos[π - φ + x] * Sin[π - φ + x]},
  {2 i * Sin[(π + 2 ε) / 2] * Cos[π - φ + x] * Sin[π - φ + x],

```

```

Exp[-i * (pi + 2 epsilon) / 2] * (Cos[pi - phi + x]) ^ 2 +
Exp[i * (pi + 2 epsilon) / 2] * (Sin[pi - phi + x]) ^ 2}}
ccwquarter := {{Exp[i * (pi / 2 + epsilon) / 2] * (Cos[pi - rho + x]) ^ 2 +
Exp[-i * (pi / 2 + epsilon) / 2] * (Sin[pi - rho + x]) ^ 2,
2 i * Sin[(pi / 2 + epsilon) / 2] * Cos[pi - rho + x] * Sin[pi - rho + x]},
{2 i * Sin[(pi / 2 + epsilon) / 2] * Cos[pi - rho + x] * Sin[pi - rho + x],
Exp[-i * (pi / 2 + epsilon) / 2] * (Cos[pi - rho + x]) ^ 2 +
Exp[i * (pi / 2 + epsilon) / 2] * (Sin[pi - rho + x]) ^ 2}}
cw = {a, 0};
ccw = {a, 0};

waveplatesCW = (fibercw.halfcw.quartercw).cw;
waveplatesCCW = (ccwquarter.ccwhalf.ccwfiber).ccw;

Eout := alpha * waveplatesCW * Exp[NOLMphaseCW (cw.Conjugate[cw])] -
(1 - alpha) * waveplatesCCW * Exp[NOLMphaseCCW (ccw.Conjugate[ccw])]
output := Sqrt[Eout[[1]] * Conjugate[Eout[[1]]] +
Eout[[2]] * Conjugate[Eout[[2]]]] /. {y -> x}
ptc = (output / a) /. fitparms;

```

(* PROGRAM ELEMENTS *)

```

Print["Beginning simulation."]

(* Nonlinear Schroedinger equation governs propagation *)

propagation = i D[u[xi, tau], xi] +
1/2 D[u[xi, tau], {tau, 2}] + (Abs[u[xi, tau]]^2) u[xi, tau] == 0;
gainpropagation = i D[u[xi, tau], xi] + 1/2 D[u[xi, tau], {tau, 2}] +
(Abs[u[xi, tau]]^2) u[xi, tau] - gain u[xi, tau] == 0;

(* Interpolate input for Mathematica friendliness -
CONSIDER THIS THE PULSE COMING FROM THE FARADAY ISOLATOR *)

initialpulse =
Interpolation[Table[{tau, inputpulse}, {tau, -40, 40, .01}]];

(* Set up output array *)

outputpulses = Table[0, {roundtrips}];

(* ADJUST GAIN PARAMETER *)

pulseMax = Max[Table[Abs[initialpulse[tau]], {tau, -5, 5, .01}]];

Print["Determining range of gain parameter..."];

While[pulseMax <= 1.0,

```

```

gainPwr = gainPwr + 1;
gain = N[2^gainPwr];

(* ER FIBER: NLSE WITH GAIN TERM *)

Clear[u, ξ, τ];
junk =
u /. First[NDSolve[{gainpropagation, u[0, τ] == initialpulse[τ]},
  u, {ξ, 0, 2 Erlength/LDsmf}, {τ, -40, 40},
  MaxSteps → {steps, steps}]];

pulse = Interpolation[Table[
  {τ, junk[Erlength/LDsmf, τ] + gainoffset}, {τ, -40, 40, .01}]];

(* NOLM: POWER TRANSFER CURVE *)

pulse = Interpolation[Table[{τ,
  pulse[τ] (ptc /. {a → (pulse[τ] / qsmf)}), {τ, -40, 40, .01}]];

(* PROPAGATE PULSE THROUGH 15 m SMF-28 FIBER: NLSE *)

Clear[u, ξ, τ];
junk =
u /. First[NDSolve[{propagation, u[0, τ] == pulse[τ]}, u, {ξ, 0, 2
  SMFlength/LDsmf}, {τ, -40, 40}, MaxSteps → {steps, steps}]];

pulse = Interpolation[
  Table[{τ, junk[SMFlength/LDsmf, τ]}, {τ, -40, 40, .01}]];

pulseMax = Max[Table[Abs[pulse[τ]], {τ, -5, 5, .01}]]

];

Print[StringForm["Gain parameter is between `` and ``",
  2^(gainPwr - 1), 2^gainPwr]];
pulse = initialpulse; (* reset input pulse *)

(* ROUND TRIPS *)

gainPwr = gainPwr - 2;
gain = gain - 2^gainPwr;
lastGain = 1.0 gain;
lastMax = 1.0;

Do[

Clear[u, ξ, τ, cwpulse, ccwpulse,
  ccwfunc, ccwpol, sum, polarized, normalized];

(* Adaptive gain parameter *)

```

```

pulseMax = Max[Table[Abs[pulse[τ]], {τ, -5, 5, .01}]];
gainPwr = If[(pulseMax ≥ 1.5 lastMax) || (pulseMax ≤ .9 lastMax),
  gainPwr - 1, gainPwr];
gain = N[If[pulseMax ≥ 1.5 lastMax,
  (lastGain - 2^gainPwr), lastGain]];
gain = N[If[pulseMax ≤ .9 lastMax, (lastGain + 2^gainPwr), gain]];
lastGain = gain;
lastMax = pulseMax;

(* ER FIBER: NLSE WITH GAIN TERM *)

Clear[u, ξ, τ];
junk = u /.
  First[NDSolve[{gainpropagation, u[0, τ] == pulse[τ]}, u, {ξ, 0,
    2 Erlength/LDsmf}, {τ, -40, 40}, MaxSteps → {steps, steps}]];

pulse = Interpolation[Table[
  {τ, junk[Erlength/LDsmf, τ] + gainoffset}, {τ, -40, 40, .01}]];

(* NOLM: POWER TRANSFER CURVE *)

pulse =
  Interpolation[Table[{τ, pulse[τ] (ptc /. {a → (pulse[τ] / qsmf)}),
    {τ, -40, 40, .01}]];

(* PROPAGATE PULSE THROUGH 15 m SMF-28 FIBER: NLSE *)

Clear[u, ξ, τ];
junk =
  u /. First[NDSolve[{propagation, u[0, τ] == pulse[τ]}, u, {ξ, 0,
    2 SMFlength/LDsmf}, {τ, -40, 40}, MaxSteps → {steps, steps}]];

pulse = Interpolation[
  Table[{τ, junk[SMFlength/LDsmf, τ]}, {τ, -40, 40, .01}]];

(* OUTPUT COUPLER *)

outputpulses[[i]] = pulse;
Print[StringForm["Round trip `` complete. Gain: ``", i, gain]],

{i, roundtrips}]

Print["*** SIMULATION COMPLETE. ***"]

Beginning simulation.

Determining range of gain parameter...

Gain parameter is between 512 and 1024

Round trip 1 complete. Gain: 768.`

Round trip 2 complete. Gain: 640.`

```

Round trip 3 complete. Gain: 704.ˆ

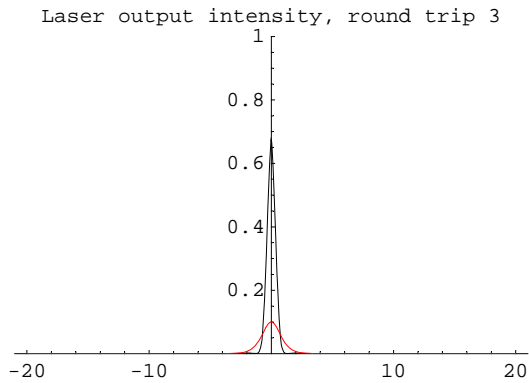
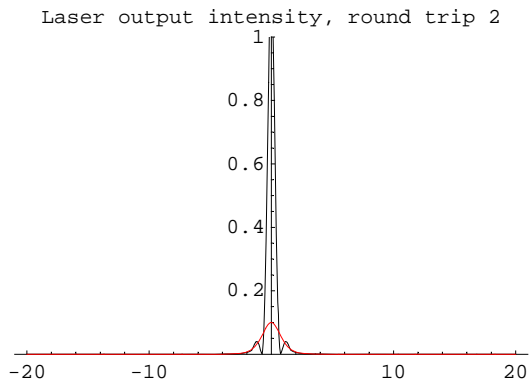
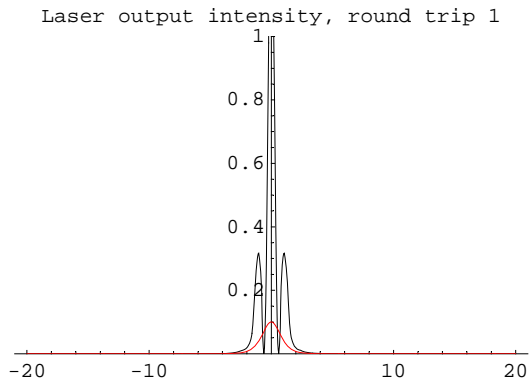
...

Round trip 50 complete. Gain: 752.ˆ

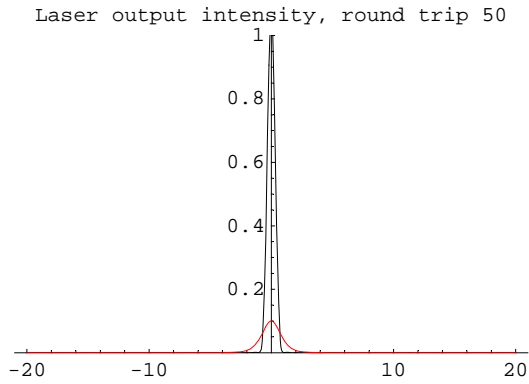
*** SIMULATION COMPLETE. ***

(* PLOT RESULTS *)

```
Do[Plot[.1 Abs[outputpulses[[i]][τ]]^2, .1 Abs[inputpulse]^2,
{τ, -20, 20}, PlotRange → {0, 1},
PlotStyle → {Black, Red}, PlotLabel → StringForm[
"Laser output intensity, round trip ``", i]], {i, roundtrips}]
```



...



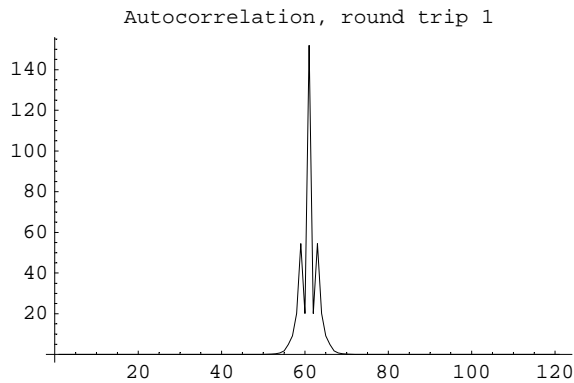
(* SIMULATE AUTOCORRELATIONS *)

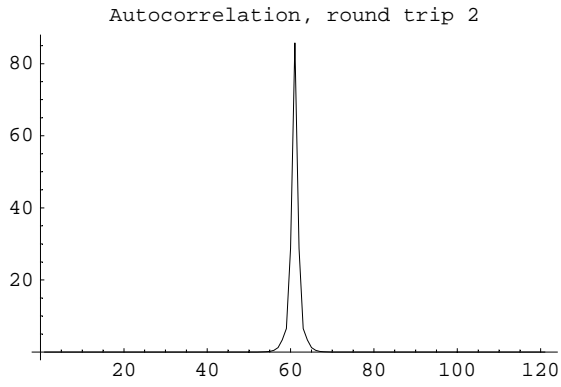
```
Clear[i, j];
```

```
delta = .5; (* spacing for "data points" *)
```

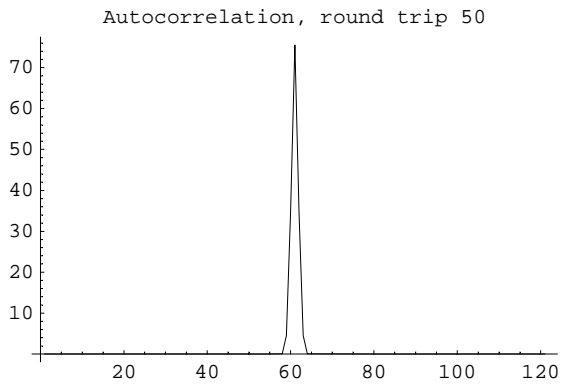
```
range = 30; (* range of autocorrelation *)
```

```
Do[ListPlot[Table[Sum[delta Evaluate[Abs[outputpulses[[n]][j]]^2
    Abs[outputpulses[[n]][i+j]]^2], {j, -range, range, delta}],
    {i, -range, range, delta}], PlotRange -> All,
    PlotLabel -> StringForm["Autocorrelation, round trip ``", n],
    PlotJoined -> True], {n, roundtrips}]
```





...



(* AVERAGE AUTOCORRELATION *)

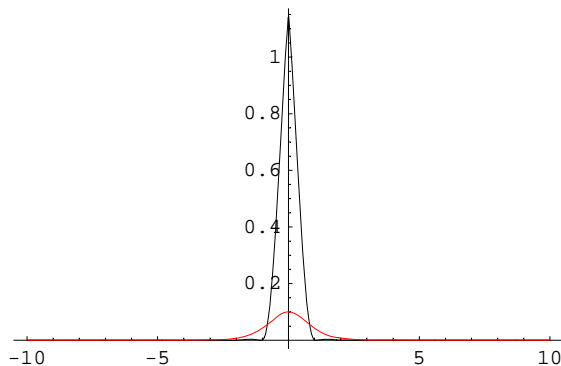
```

Clear[i, j];

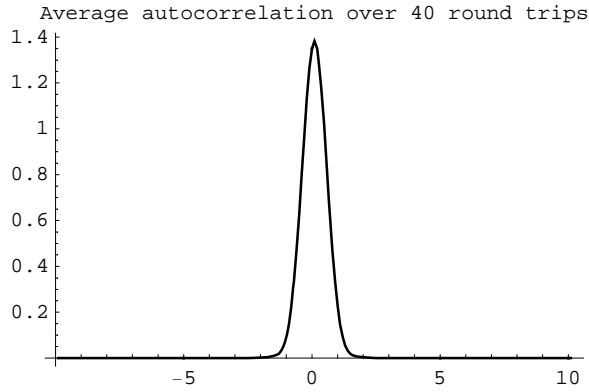
delta = .1; (* spacing for "data points" *)
range = 10; (* range of autocorrelation *)
jitter = 0;
(* max timing jitter for simulating experimental error *)
steady = 10; (* number of round trips
after which pulse achieves steady state *)

avgpulse = Interpolation[
  Table[{ $\tau$ , Sum[outputpulses[[i + steady]][ $\tau$ ] / (roundtrips - steady),
    {i, roundtrips - steady}]}], { $\tau$ , -40, 40}]]
Plot[ {.1 Abs[avgpulse[ $\tau$ ]]^2, .1 Abs[inputpulse]^2},
  { $\tau$ , -range, range}, PlotRange  $\rightarrow$  All,
  PlotStyle  $\rightarrow$  {Black, Red}, PlotLabel  $\rightarrow$ 
  StringForm["Average laser output intensity for `` round trips",
    roundtrips - steady]]
autocorrelation = Table[
  Sum[delta Evaluate[Abs[avgpulse[j]]^2 Abs[avgpulse[
    i + j + Random[Real, {-jitter, jitter}]]]^2] / roundtrips,
  {j, -range, range, delta}], {i, -range, range, delta}];
autoplot = ListPlot[
  autocorrelation, PlotRange  $\rightarrow$  All,
  PlotStyle  $\rightarrow$  {PointSize[0.015], Thickness[0.005]}, PlotLabel  $\rightarrow$ 
  StringForm["Average autocorrelation over `` round trips",
    roundtrips - steady], PlotJoined  $\rightarrow$  True,
  Ticks  $\rightarrow$  {{0, "-10"}, {10, ""}, {20, ""}, {30, ""}, {40, ""},
    {50, "-5"}, {60, ""}, {70, ""}, {80, ""}, {90, ""}, {100, "0"},
    {110, ""}, {120, ""}, {130, ""}, {140, ""}, {150, "5"}, {160, ""},
    {170, ""}, {180, ""}, {190, ""}, {200, "10"}}, Automatic]]
Average laser output intensity for 40 round trips

```



- Graphics -

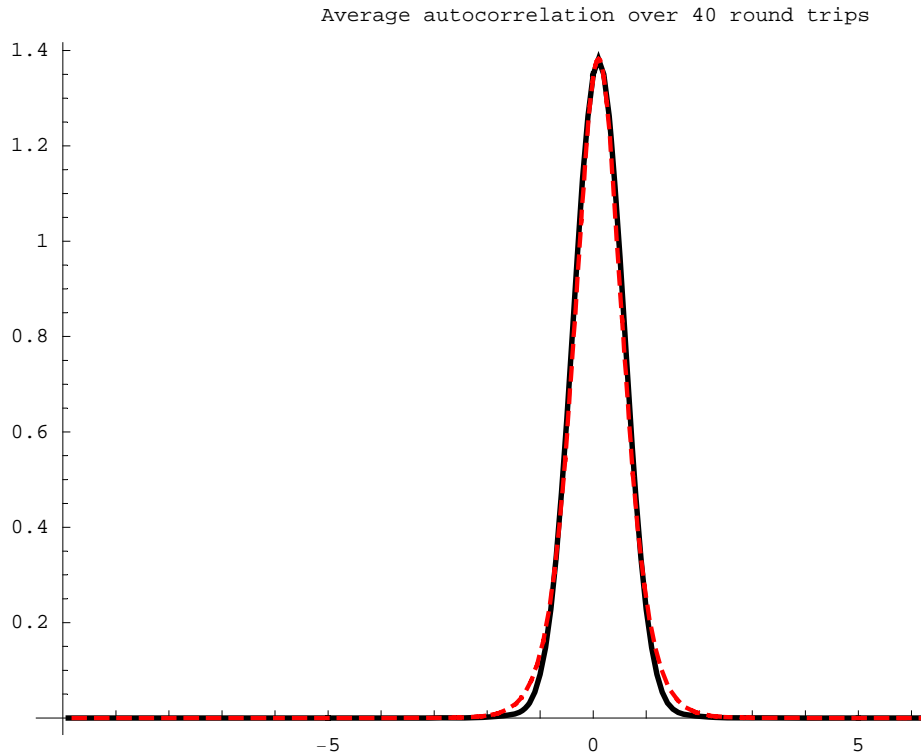


- Graphics -

(* Kluge together simulated
autocorrelation and a Sech² for comparison *)

```
soliton = Max[autocorrelation]
  Sech[(t - First[First[Position[autocorrelation,
    Max[autocorrelation]]]]) / 6]^2;
solplot = Plot[soliton, {t, 0, 200}, PlotRange -> All,
  PlotStyle -> {Dashing[ {.01, .01}], Thickness[.004], Red},
  DisplayFunction -> Identity]
Show[autoplot, solplot, DisplayFunction -> $DisplayFunction]
```

- Graphics -



- Graphics -

```
(* Figure out simulated autocorrelation FWHM *)

NSolve[Abs[soliton] == Abs[Max[autocorrelation] / 2], t]

{{t -> 95.7118}, {t -> 95.7118 - 18.8496 i},
 {t -> 106.288}, {t -> 106.288 + 18.8496 i}}

delta (106.28824152211726` - 95.71175847788274`)

1.05765

(* Figure out simulated pulse FWHM *)

solitontable = Table[Abs[avgpulse[tau]]^2, {tau, -range, range, delta}];
delta First[
  (Last[Position[solitontable, _? (# >= (Max[solitontable] / 2) &)]] -
   First[Position[solitontable,
     _? (# >= (Max[solitontable] / 2) &)]])]

0.6

(* This is the ratio of the two *)

1.0576483044234521` / 0.6000000000000001`

1.76275
```